AD-A061 570 NAVAL OCEAN SYSTEMS CENTER SAN DIEGO CA F/G 20/14
EFFECTS OF STRONG LOCAL SPORADIC E ON ELF PROPAGATION.(U)
AUG 78 R A PAPPERT, L R SHOCKEY
UNCLASSIFIED NOSC/TR-282 NL

| OF |
AD
A061570

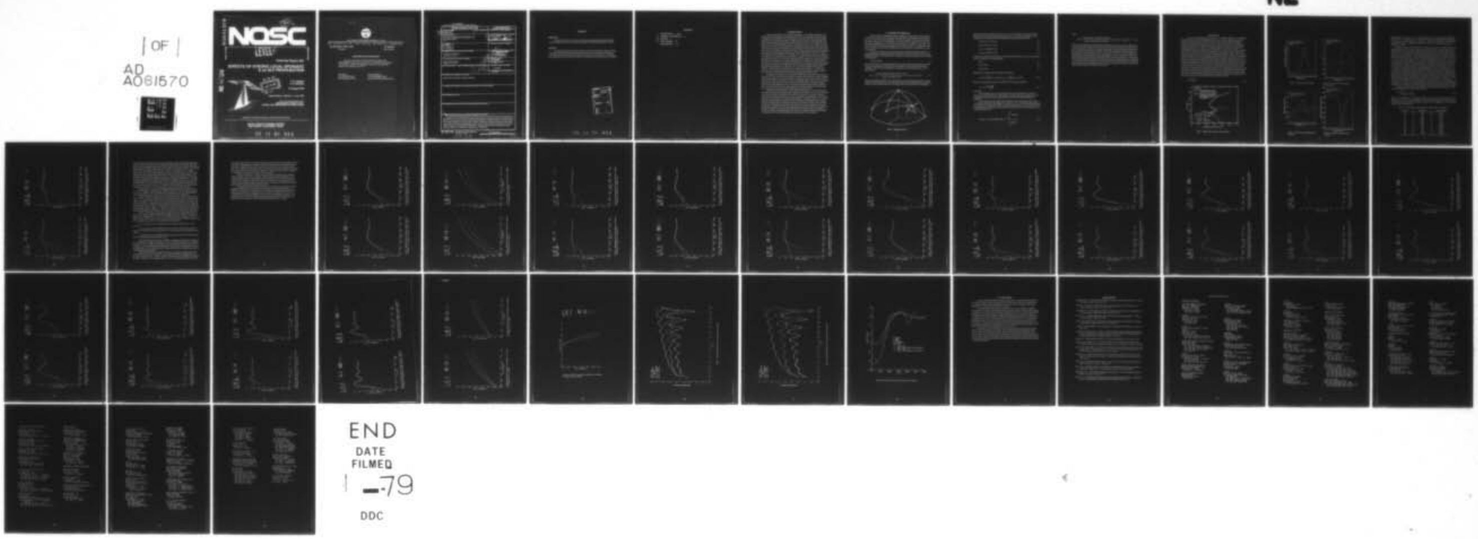

END
DATE
FILMED
1 -79
DDC

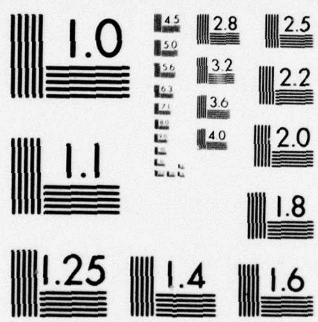

MICROCOPY RESOLUTION TEST CHART
NATIONAL BUREAU OF STANDARDS-1963-A

AD A061570

NOSC

LEVEL II

NOSC TR 282

NOSC TR 282

Technical Report 282

EFFECTS OF STRONG LOCAL SPORADIC E on ELF PROPAGATION

DDC FILE COPY

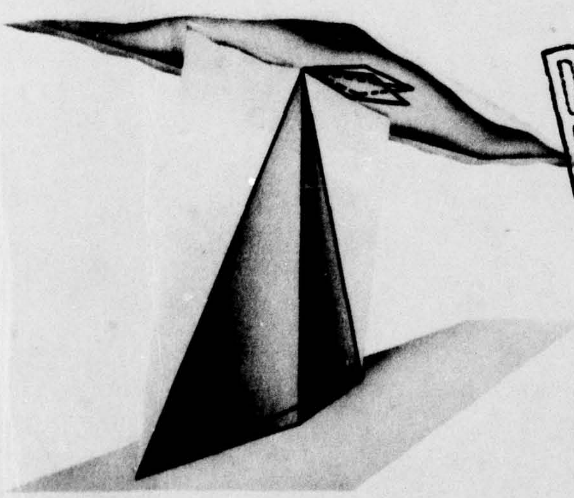

D D C
RECEIVED
NOV 27 1978
F

R. A. Pappert
L. R. Shockey

15 August 1978

Interim Report: 1 February – 1 June 1978

This work sponsored by the
Defense Nuclear Agency under
Subtask Code S99QAXHB051 and Work Unit 08

APPROVED FOR PUBLIC RELEASE; DISTRIBUTION UNLIMITED

NAVAL OCEAN SYSTEMS CENTER
SAN DIEGO, CALIFORNIA 92152

78 11 22 011

NAVAL OCEAN SYSTEMS CENTER, SAN DIEGO, CA 92152

AN ACTIVITY OF THE NAVAL MATERIAL COMMAND

RR GAVAZZI, CAPT, USN
Commander

HL BLOOD
Technical Director

ADMINISTRATIVE INFORMATION

This work, sponsored by the Defense Nuclear Agency under S99QAXHB051 work unit 08, was done by the Nuclear Effects Branch during the period 1 February 1978 through 1 June 1978. The report was approved for publication July 1978.

Released by
J. H. RICHTER, Head
EM Propagation Division

Under authority of
J. D. HIGHTOWER, Head
Environmental Sciences Department

UNCLASSIFIED

SECURITY CLASSIFICATION OF THIS PAGE (When Data Entered)

REPORT DOCUMENTATION PAGE		READ INSTRUCTIONS BEFORE COMPLETING FORM
1. REPORT NUMBER 14 NOSC/TR-282	2. GOVT ACCESSION NO.	3. RECIPIENT'S CATALOG NUMBER
4. TITLE (and Subtitle) 6 EFFECTS OF STRONG LOCAL SPORADIC E ON ELF PROPAGATION.		5. TYPE OF REPORT & PERIOD COVERED 9 Interim Report. 1 Feb[redacted] – 1 Jun[redacted]78, 6. ~~PERFORMING ORG. REPORT NUMBER~~
7. AUTHOR(s) 10 R. A. Pappert L. R. Shockey		8. CONTRACT OR GRANT NUMBER(s) 16
9. PERFORMING ORGANIZATION NAME AND ADDRESS Naval Ocean Systems Center San Diego, CA 92152		10. PROGRAM ELEMENT, PROJECT, TASK AREA & WORK UNIT NUMBERS 6.27.04H/S99QAXH 17 B051 532-MP20B/08ELF
11. CONTROLLING OFFICE NAME AND ADDRESS Defense Nuclear Agency Washington, DC 20350	11 15	12. REPORT DATE Augu[redacted]78 13. NUMBER OF PAGES 34
14. MONITORING AGENCY NAME & ADDRESS (if different from Controlling Office) 12 43p.		15. SECURITY CLASS. (of this report) Unclassified 15a. DECLASSIFICATION/DOWNGRADING SCHEDULE

16. DISTRIBUTION STATEMENT (of this Report)

Approved for public release; distribution unlimited.

17. DISTRIBUTION STATEMENT (of the abstract entered in Block 20, if different from Report)

18. SUPPLEMENTARY NOTES

19. KEY WORDS (Continue on reverse side if necessary and identify by block number)

20. ABSTRACT (Continue on reverse side if necessary and identify by block number)

A simple Kirchhoff-Huygens diffraction model has been used to estimate the effect of a patch of sporadic E on propagation in the lower ELF band. The patch is approximated by a lumped parameter phase-amplitude screen allowed to move along a great circle path normal to the transmitter-receiver great circle path. The results indicate that sporadic E patches on the order of 1000 X 1000 km, causing phase rate shifts and attenuation rate enhancements consistent with full wave modal evaluations, can account for the 6–8 dB fades observed in connection with 1600 km Wisconsin Test Facility (WTF) transmissions. The results suggest also that such disturbances can be expected to produce 2 to 4 dB fades over paths as long as 10,000 km.

DD FORM 1 JAN 73 1473 EDITION OF 1 NOV 65 IS OBSOLETE

S/N 0102-014-6601 |

UNCLASSIFIED

SECURITY CLASSIFICATION OF THIS PAGE (When Data Entered)

393 159

SUMMARY

OBJECTIVE

Determine the effects of off path ionospheric inhomogeneities (sporadic-E patches) on the propagation of ELF waves by using a simple Kirchhoff-Huygens diffraction model.

RESULTS

The results indicate that sporadic E patches of the order 1000 km by 1000 km which cause phase shifts and attenuation rate increases can account for the 6–8 dB fades observed over 1600 km transmission paths from the Navy's Wisconsin Test Facility ELF Transmitter. Such disturbances can be expected to produce 2 to 4 dB fades over paths as long as 10,000 km.

ACCESSION for
NTIS White Section ☑
DDC Buff Section ☐
UNANNOUNCED ☐
JUSTIFICATION
BY
DISTRIBUTION/AVAILABILITY CODES
Dist. SPECIAL
A

78 11 22 011

CONTENTS

I. INTRODUCTION . . . page 3
II. SUMMARY OF FORMULAS . . . 4
III. RESULTS . . . 7
IV. CONCLUSIONS . . . 33
BIBLIOGRAPHY . . . 34

I. INTRODUCTION

In recent works (Barr, 1977; Pappert and Shockey, 1978; Pappert and Moler, to be published) it has been suggested that nighttime sporadic E layering could produce an order of magnitude enhancement of the earth ionosphere waveguide attenuation rate and thereby account for the 6 to 8 dB short path ($\cong$ 1600 km) fades reported in connection with transmissions from the Wisconsin Test Facility (WTF) (Davis and Meyers, 1975; Bannister, 1975; Davis, 1976). Since the signal from a remote transmitter is received over a range of azimuth angles, the extent of the effect produced by sporadic-E layering depends among other things, upon the size and shape of the disturbance, its proximity to the transmitter or receiver terminals, and its location relative to the great circle path. Although several authors have addressed the question of off path effects (Crombie, 1963; Wait, 1964a, 1964b; Galejs, 1971; Wilcox, 1974; Greifinger and Greifinger 1977; Shellman, 1977), principally on the basis of theoretical development, to the present authors' knowledge no computer code exists which can handle in generality the problem of off path effects associated with propagation in a spherical geometry with simultaneous allowance for vertical inhomogeneity and anisotropy of the ionosphere. Therefore, to obtain at least a semiquantitative estimate of the effect on signal level produced by sporadic E layering we use in this study, because of ease of implementation, a Kirchhoff-Huygens diffraction model (e.g., Marcuse, 1972). The model is similar to that used by Crombie. Unlike Crombie's work however, the Fresnel approximation to the diffraction integral is not invoked but rather the diffraction integral is evaluated by numerical integration. The latter is preferable because of the long wavelengths involved at ELF.

Propagation is assumed to occur along the surface of the earth and the disturbance is modeled by a screen, endowed with attenuation and phase shift properties, which is imagined to move along a great circle contour transverse to the great circle path connecting transmitter and receiver. Effort is concentrated on screens of 1000 km length. This seems to be a reasonable upper limit since the spectrum of reported lateral dimensions of sporadic E layering ranges to that order (Whitehead, 1970). Attenuation and phase shift properties assigned to the screen are selected to be in the range indicated by full wave solutions for ELF propagation in a laterally uniform guide with a superimposed sporadic E layer.

Basically the phase amplitude screen concept is tantamount to the assumption that although the sporadic E disturbance is three dimensional, its effect can be crudely represented by a lumped attenuation and phase shift bounded in the direction transverse to the great circle path connecting transmitter and receiver by the edges of the disturbance. Merit of the model as used in this study is its ease of implementation. Although we believe it is useful for predicting trends and giving an indication of the dependence of signal level on the size and location of the disturbance as well as pointing out the importance of phase shift in addition to attenuation enhancement associated with a disturbance, the model should in no way be construed as a substitute for a full wave treatment of the problem. Rather, the magnitude of the effect indicated in the present study fully supports the need for full wave algorithms capable of handling two dimensional lateral variations in a spherical geometry with simultaneous allowance for vertical inhomogeneity and anisotropy of the ionosphere.

II. SUMMARY OF FORMULAS

Figure 1 shows the essential geometry consisting of a transmitter at 0 and receiver at P. A, B, $A + \delta_1$, $B + \delta_2$, and Y are great circle arcs and their central angles will be denoted by $\hat{a}$, $\hat{b}$, $\hat{a} + \hat{\delta}_1$, $\hat{b} + \hat{\delta}_2$, and $\hat{y}$ respectively. P′ represents a point on the great circle contour QQ′ which is transverse to the transmitter receiver path OP and a distance Y from the latter. The phase amplitude screen to be introduced is assumed to lie along the contour QQ′. The great circle arc SS′ is transverse to the great circle arc QQ′ at point P′. The angles of intersection of the great circle arc SP′ with the great circle arcs PP′ and OO′ are denoted by γ_1 and γ_2 respectively.

The point of departure for the present study is the Kirchhoff-Huygens diffraction integral along with the assumption that the channeled wave at P′ due to 0 and the wave at P reradiated from P′ are both described by an asymptotic outgoing Legendre function. Roughly this requires that

$$A, B \geqslant \lambda/(2\pi|S|) \tag{1}$$

where λ is the free space wavelength and S the sine of the complex eigenangle for the TEM (the only nonevanescent mode) mode which propagates at ELF in the earth ionosphere waveguide. Thus, the crucial assumption is made that the unperturbed field, E_{zo}, at P is proportional to

$$E_{zo} \sim \int_C \frac{\exp[-(\gamma/8.68 + i\omega/v)(A + B + \delta_1 + \delta_2)]}{[\sin(\hat{a} + \hat{\delta}_1)\sin(\hat{b} + \hat{\delta}_2)]^{1/2}} (\cos\gamma_1 + \cos\gamma_2)\, dY \tag{2}$$

where C is the great circle QQ′, γ is an attenuation rate for the ambient guide and v a phase velocity for the ambient guide. Such subtleties as spatial or directional dependencies of those quantities as well as mode reflection or conversion due to lateral variation are completely

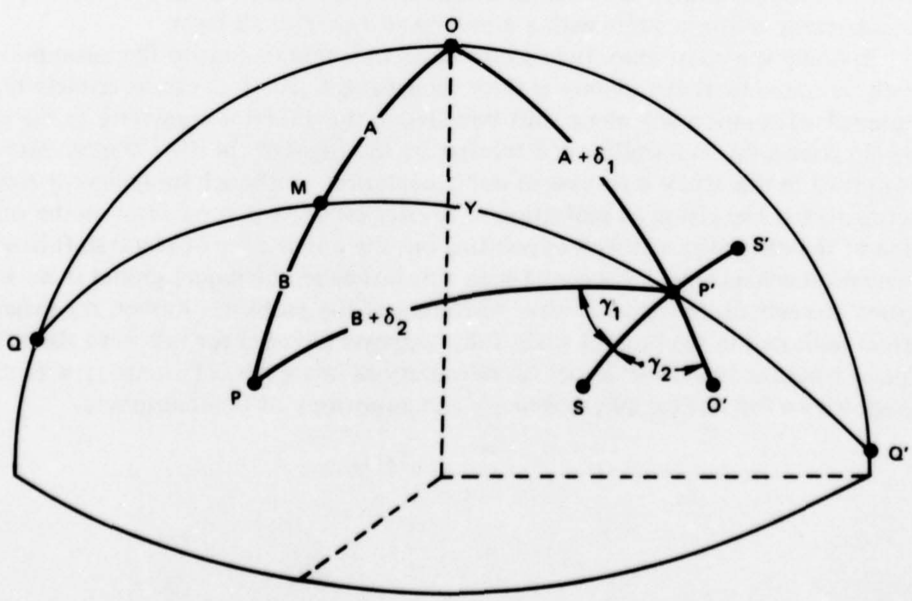

Figure 1. Propagation geometry.

ignored in this study. Observe that $(\cos\gamma_1 + \cos\gamma_2)$ is an obliquity factor and that the Y dependence enters into the integrand through the $\delta_1, \delta_2, \gamma_1$, and γ_2 dependencies. These dependencies are obtained from the following spherical trigonometric formulas:

$$\cos(\hat{a} + \hat{\delta}_1) = \cos\hat{y}\cos\hat{a} \tag{3}$$

$$\cos(\hat{b} + \hat{\delta}_2) = \cos\hat{y}\cos\hat{b} \tag{4}$$

$$\cos\gamma_1 = \sin\hat{a}/\sin(\hat{a} + \hat{\delta}_1) \tag{5}$$

$$\cos\gamma_2 = \sin\hat{b}/\sin(\hat{b} + \hat{\delta}_2) \tag{6}$$

In practice $\hat{\delta}_1$ and $\hat{\delta}_2$ are found from (3) and (4), respectively and $\cos(\gamma_1, \gamma_2)$ is found from (5) or (6). Subject to the approximations

$$\hat{y} \ll 1 \tag{7}$$

$$\hat{\delta}_1 \ll 2\tan\hat{a} \tag{8}$$

$$\hat{\delta}_2 \ll 2\tan\hat{b}, \tag{9}$$

Equations (3) and (4) lead to a result given by Crombie:

$$\hat{\delta}_1 + \hat{\delta}_2 \cong \frac{\hat{Y}^2}{2}(\cot\hat{a} + \cot\hat{b}) \text{ or } \delta_1 + \delta_2 \cong \frac{Y^2}{2r}(\cot\hat{a} + \cot\hat{b}) \tag{10}$$

where r is the radius of the earth. In the limit $\hat{a}, \hat{b} \ll 1$, the flat earth limit

$$\delta_1 + \delta_2 \cong \frac{Y^2}{2}\frac{A+B}{AB} \tag{11}$$

is retrieved.

The attenuation rate, γ, and the obliquity factor in the integrand of (2) tend to reduce the off path contributions. With allowance for these factors it is expected that off path effects will damp out more rapidly than they would were Fresnel filtering alone considered.

Now suppose that the fictitious phase amplitude screen falls along the great circle contour QQ′ between the limits (edges) Y_1 and Y_2 $(Y_2 > Y_1)$ and that the screen introduces an "enhanced" attenuation β (in dB) and an additional phase shift ϕ. Then according to the crucial assumption of Equation (2) the ratio of the perturbed (by the screen) field, E_z, to the unperturbed field will be

$$E_z/E_{zo} \cong 1 + (\exp(-\beta/8.68 - i\phi) - 1)\;\frac{\int_{Y_1}^{Y_2} F(Y)dY}{\int_c F(Y)dY} \tag{12}$$

where

$$F(Y) = \frac{\exp[(-\gamma/8.68 - i\omega/v)(\delta_1(Y) + \delta_2(Y))]}{[\sin(\hat{a} + \hat{\delta}_1(Y)) \sin(\hat{b} + \hat{\delta}_2(Y))]^{1/2}} (\cos(\gamma_1(Y)) + \cos(\gamma_2(Y))) \tag{13}$$

Clearly, the attenuation, β, and phase shift, ϕ, properties of the screen could be allowed to be a function of position along the screen (Y) and the associated terms retained within the integral. This might be desirable; for example, if modeling for a specifically shaped perturbation, say circular, allowance could be provided for the different lengths of travel through the perturbed regions. If the attenuation "rate" and phase shift "rate" were constant through the perturbed region then the β and ϕ would be proportional to the travel lengths and this could quite easily be accommodated with the model. Where to place the screen (i.e., what value of A to use) would remain a question best answered probably in empirical fashion by comparing with a selection of full wave results. In the present study such refinements are not attempted and all results given in the following section are based on Equation (12) which in turn is predicated on the constancy of β and ϕ over the screen.

III. RESULTS

In previous studies (Pappert and Shockey, 1977; Pappert and Moler, to be published) full wave outputs for an ambient nighttime profile and an ambient nighttime profile disturbed by a sporadic E layer (see Figure 2) have been analyzed as regards ionospheric absorption and reflection features of ELF waves. Figures 3 through 6 show comparisons between ambient and the ambient plus sporadic E modal properties and excitations in the frequency range from 45 to 100 Hz. In particular Figure 3 shows the attenuation rate (dB/1000 km), Figure 4 the phase velocity normalized to the free space velocity c, Figures 5 and 6 show the magnitude and phase respectively for the vertical E field excitation factor produced by end-on launch from a ground based horizontal dipole. Figure 3 illustrates the distinct possibility of an order of magnitude enhancement of the attenuation rate associated with the sporadic E layer and Figure 4 illustrates the possibility of substantial phase shift. Figures 5 and 6 illustrate the likelihood that should the sporadic E disturbance pass over the terminals, additional effects due to excitation factor fluctuations could be expected. However, effects attributable to the latter are not considered further in this study but certainly should be allowed for in full wave treatments. The subsequent plots are based on modal parameters consistent with those shown in Figures 3 and 4. Specifically, plots are shown for a number of transmitter receiver distances (denoted by D on the plots) for several values of beta and phi showing among other things signal variation with location of the phase amplitude screen on the great circle path transverse to the great circle path connecting the transmitter and receiver. The latter position is denoted by the midpoint

$$Y = \frac{Y_1 + Y_2}{2} \tag{14}$$

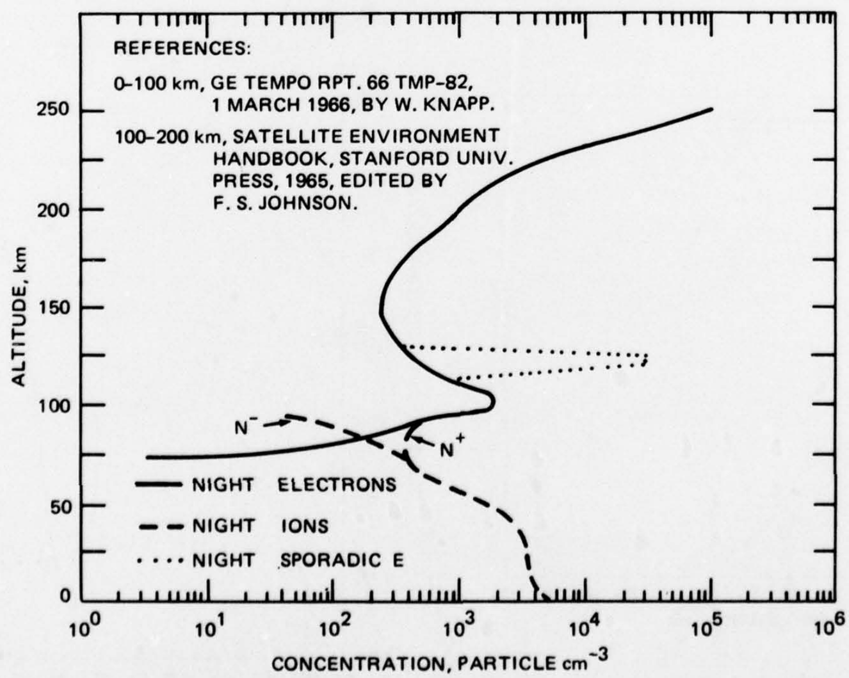

Figure 2. Night ambient profile and night sporadic E.

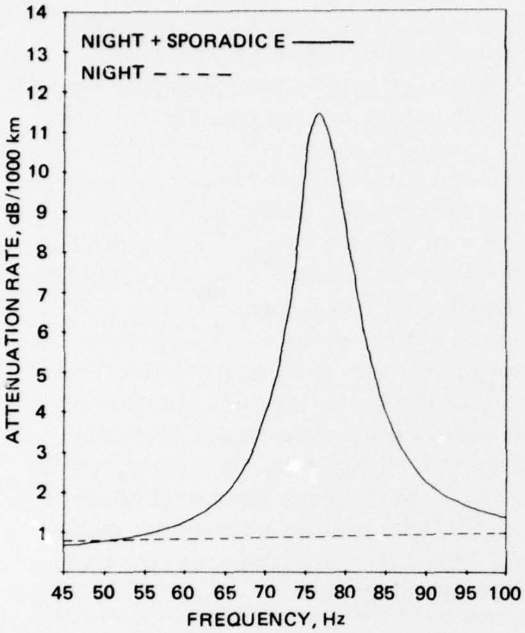

Figure 3. Attenuation versus frequency.

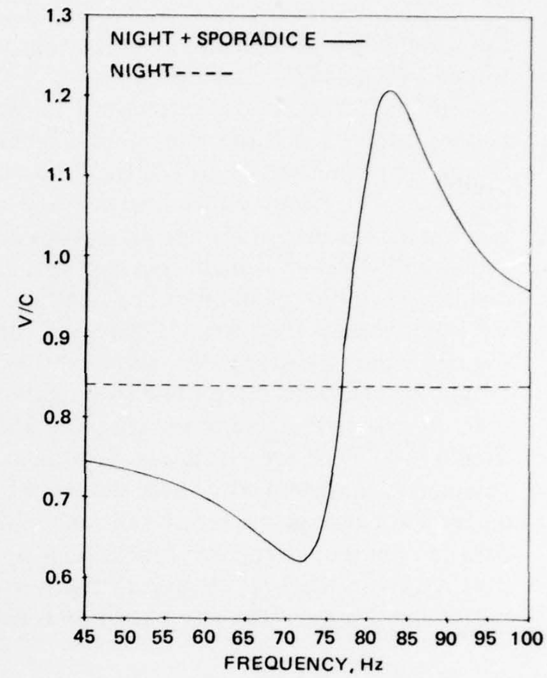

Figure 4. Phase speed over free space speed versus frequency.

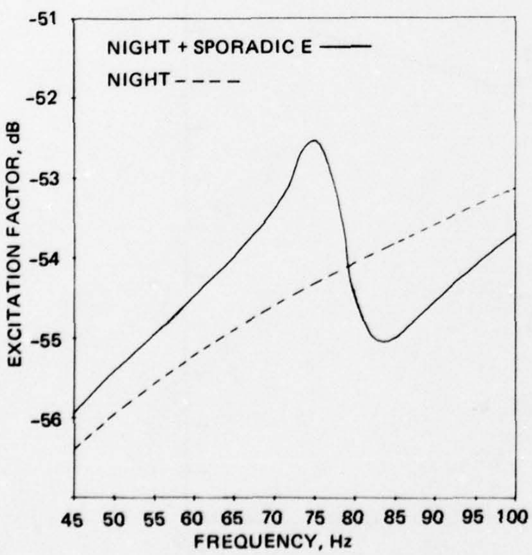

Figure 5. Excitation factor magnitude versus frequency.

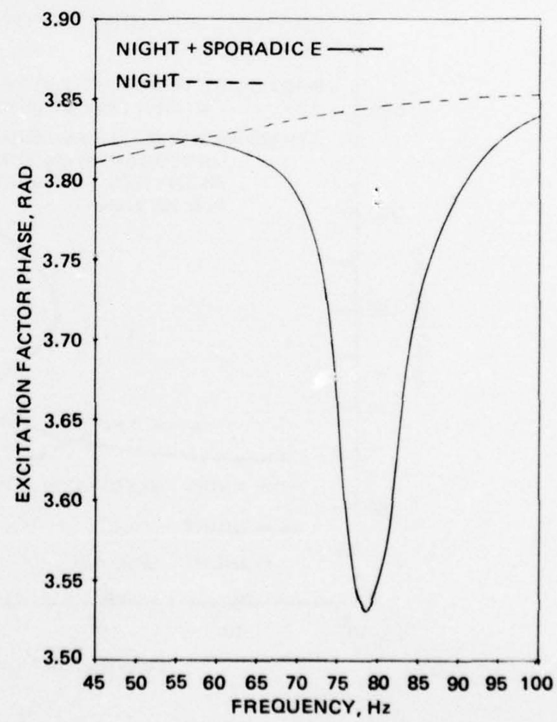

Figure 6. Excitation factor phase versus frequency.

and the length of the screen (i.e., $Y_2 - Y_1$) is denoted by T. Several values for the position of the screen, A, (see Figure 1) are considered and it should be realized that the interchange of A, B leave the result invariant (e.g., the case A = 1000 km, B = 5000 km is mathematically identical to the case A = 5000 km, B = 1000 km). All of the subsequent figures are for a frequency of 75 Hz.

Figures 7 through 16 show results for a 1600 km path since 6 to 8 dB fades have been reported for paths of that length. Figures 7 and 8 show results for a screen length equal to 1000 km since the spectrum of lateral dimensions of sporadic E have been reported to that order. Shown on each figure are results for the field perturbation, in dB (Equation (12)) as a function of the center position of the screen (Equation (14)). Results are shown for total attenuation enhancement of 1, 5, and 10 dB and both figures are for a zero phase shift screen (i.e., $\phi = 0$). Since the magnitude of the sine of the eigenangle (S), is typically in the range of 1.2, the smallest possible value of "A" consistent with the condition given in Equation (1) is 500 km and such a small value is marginal indeed. Nonetheless, in Figure 7 results are given for this value and in Figure 8 results are given for the midpoint value of 800 km. It will be seen that the fading in this instance is only slightly greater for A = 500 km than it is for A = 800 km. To approach even the reported 6 dB figure for fadings, it is clear that an order of magnitude enhancement in the attenuation is required for the parameters appropriate to Figures 7 and 8. Maximum fading occurs when the perturbation screen is centered about the great circle path connecting transmitter and receiver and the deviation from ambient is less than 0.5 dB for off path locations of the mid-point of the screen greater than about 1700 km. According to Equation (10) the first Fresnel zone size is 1079 km for A = 500 km and 1165 km for A = 800 km. The outer boundary of the second Fresnel zone is $\sqrt{2}$ times these. The off path factors allowed for in the integrand of Equation (12) tend to damp the off path oscillations more rapidly than would have been the case had Fresnel filtering been employed.

Figures 3 and 4 illustrate the possibility of a substantial attenuation and phase shift occurring simultaneously. Table 1 shows the value

$$\psi = \frac{2\pi f}{c}\left[\frac{1}{(v/c)_d} - \frac{1}{(v/c)}\right] \tag{15}$$

where "f" is the frequency, "c" the speed of light in vacuum, and v the phase velocity. The subscripts "d" and "a" stand for "disturbed" and "ambient," respectively. The table shows the results for the rate of phase retardation or advance in the neighborhood of the resonance along with the attenuation rate.

Table 1. Attenuation rate and rate of phase change close to resonance.

Freq, Hz	dB/1000 km	degrees/1000 km
72	5.99	38.25°
73	7.31	36.85°
74	8.83	32.25°
75	10.29	23.65°
76	11.24	11.17°
77	11.38	-2.39°
78	10.81	-14.08°
79	9.82	-22.66°
80	8.71	-27.96°
81	7.55	-31.07°
82	6.48	-32.23°
83	5.50	-32.05°

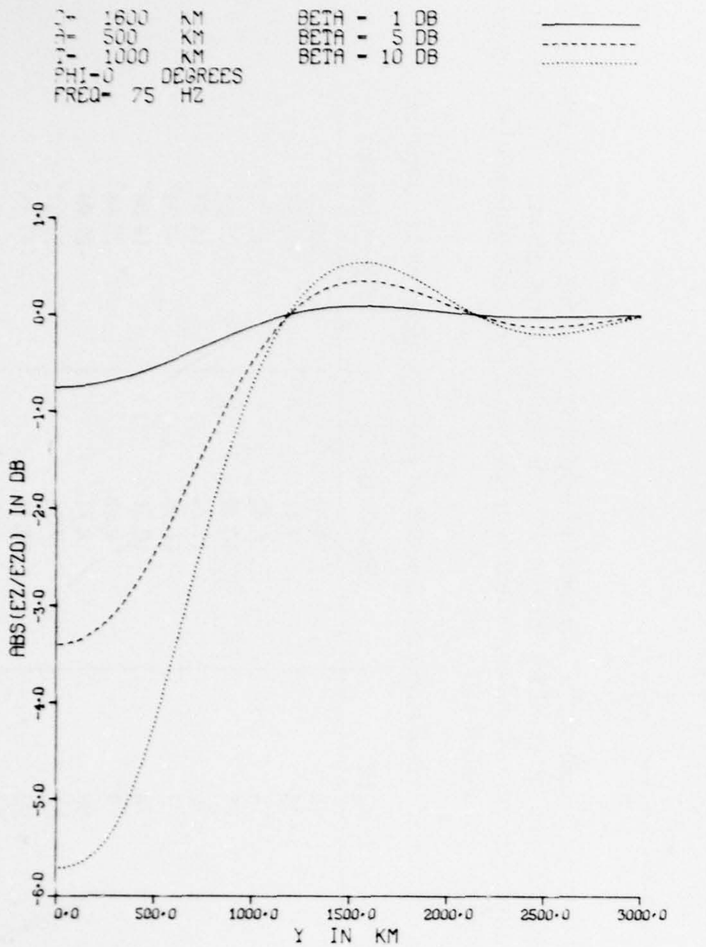

Figure 7. Signal level versus off path location (D = 1600 km, A = 500 km, T = 1000 km, β = 1, 5, 10 dB, ϕ = 0°).

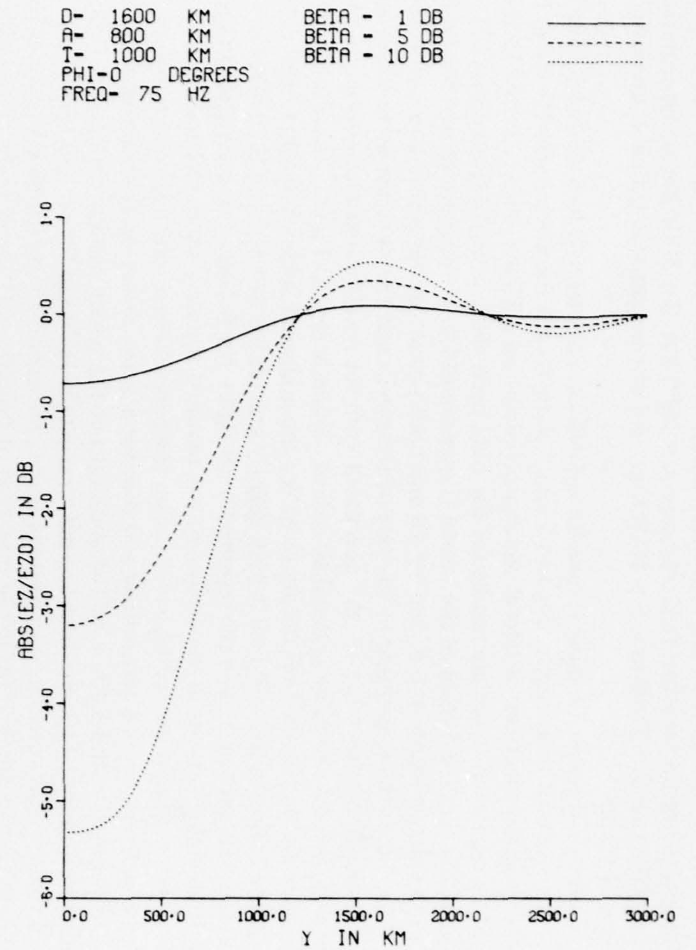

Figure 8. Signal level versus off path location (D = 1600 km, A = 800 km, T = 1000 km, β = 1, 5, 10 dB, ϕ = 0°).

An examination of the table shows that for a disturbance which extends 1000 km along the guide, it is quite within reason that an attenuation enhancement of 8 dB along with a 30° phase change can simultaneously occur. Thus, Figures 9 and 10 show results for the 1600 km path with a screen length equal to 1,000 km for values of ϕ (Equation (12)) of –30°, 0°, 30° and β = 8 dB. In particular, Figure 9 is for A = 500 km and Figure 10 for A = 800 km. Again, there is not a great deal of difference between the results for the two A values. The significant feature is that the signal level for the –30° case is down about another 1.5 dB from the results indicated in Figures (7) and (8) and definitely within the 6 to 8 dB range quoted in connection with the WTF transmissions to Connecticut and Maryland. As before, the phase-amplitude screen effects damp out when the midpoint of the screen exceeds the outer boundary of the second Fresnel zone. Also, note that the minimum signal level for ϕ = 30° occurs not for Y = 0 but for Y $\cong$ 400 km. The latter feature, that is the minimum signal level occurring for Y $\neq$ 0, is common to a number of the subsequent curves.

Figures 11 and 12 show, for the 1600 km path, signal level as a function of ϕ for β = 6, 8 and 10 dB and a screen length of 1,000 km. Figure 11 is for A = 500 km and Figure 12 for A = 800 km. The curves illustrate the significance of the phase shift although it must be remembered that ϕ and β are not, as discussed previously, independent.

Figures 13 through 16 show results for the 1600 km path but with a screen length of 500 km. Since the screen is intended here as a lumped parameter model of a sporadic E disturbance of roughly 500 by 500 km, the total attenuation and phase shifts are halved from their previous values. Examination of the figures indicates that disturbances on that spatial scale even with order of magnitude enhancement of the attenuation rate cannot explain the 6 to 8 dB fades reported. Thus, in the subsequent figures the screen thickness is assigned the reasonable upper value of 1000 km. As shown, this thickness coupled with an order of magnitude enhancement of the attenuation rate can account for the observed short path fades.

Figures 17 through 38 show detailed off path behavior for transmitter-receiver distances, D, of 2000 km, 4000 km, 6000 km and 8000 km. For each value of D results are given for the combination ϕ = 0°, β = 1, 5, and 10 dB, and for the combination ϕ = –30°, 0°, and 30° with β = 8 dB. Also for each D value results are given for A = 500 km, 1000 km, and for the midpoint value A = D/2. The results indicate the following:

a. For each value of A the deepest fades occur with the combination ϕ = –30°, β = 8 dB.

b. For A values of 500 and 1000 km the deepest fades associated with (a) above always occur with the screen centered about the great circle path connecting transmitter and receiver.

c. The perturbation is essentially damped out when the center of the screen exceeds the outer boundary of the second Fresnel zone.

Figures 39 through 41 show for D = 8000 km the variation of signal level with ϕ for β's = 6, 8 and 10 dB. In particular, Figure 39 is for A = 500 km, Figure 40 for A = 1000 km, and Figure 41 for A = 4000 km. Although the curves indicate that the phase shift can be as important or more important than the attenuation, it must be kept in mind that the two are not independent (i.e., it is unlikely that a 45° phase shift could occur simultaneously with a 6 dB attenuation enhancement).

The major results as far as depth of the fades is concerned are conveniently summarized in Figures 42 and 43. In particular, we have plotted the deepest fades for the cases (β = 10, ϕ = 0° and β = 8, ϕ = –30°) as a function of D (going out to 16,000 km) for A values of 500 km, 1000 km, and the midpoint value A = D/2. The oscillatory nature of the curves

is a consequence of the round the world (long path) wave interfering with the diffracted short path field. This interference is probably somewhat magnified because the ambient attenuation rate of 1 dB/1000 km used in the present study is probably low for a global average. Also, the $\pi/2$ advance of the long path wave as a consequence of passage through the antipode has not been allowed for in the present calculations. Nevertheless, the results are indicative of the behavior to be expected in a more refined treatment.

Even discounting the A = 500 km case, as stretching the validity of the condition given in Equation (1) too far, and in spite of representing the oscillatory behavior of the results of Figures 42 and 43 by imaginary smooth average curves, it is clear that for ranges on the order of 10,000 km, fades in the range of 2 to 4 dB could be anticipated. Fades within the latter range have apparently been observed in connection with the WTF transmissions to Italy (John Davis private communications).

At several junctures in this report we have made reference to the fact that the total integrand of Equation (2) has been allowed for by means of numerical integration. It is legitimate to inquire into the differences to be expected if Fresnel filtering alone were considered. Figure 44 shows a comparison for D = 1600 km, A = 800 km, $\phi = 0^\circ$ and $\beta = 5$, 10 dB between the numerical integration result and the Fresnel integral calculation. The major differences are that the additional terms in the integrand tend to damp out the off path effects more rapidly and tend to stabilize the behavior in the Y = 0 range.

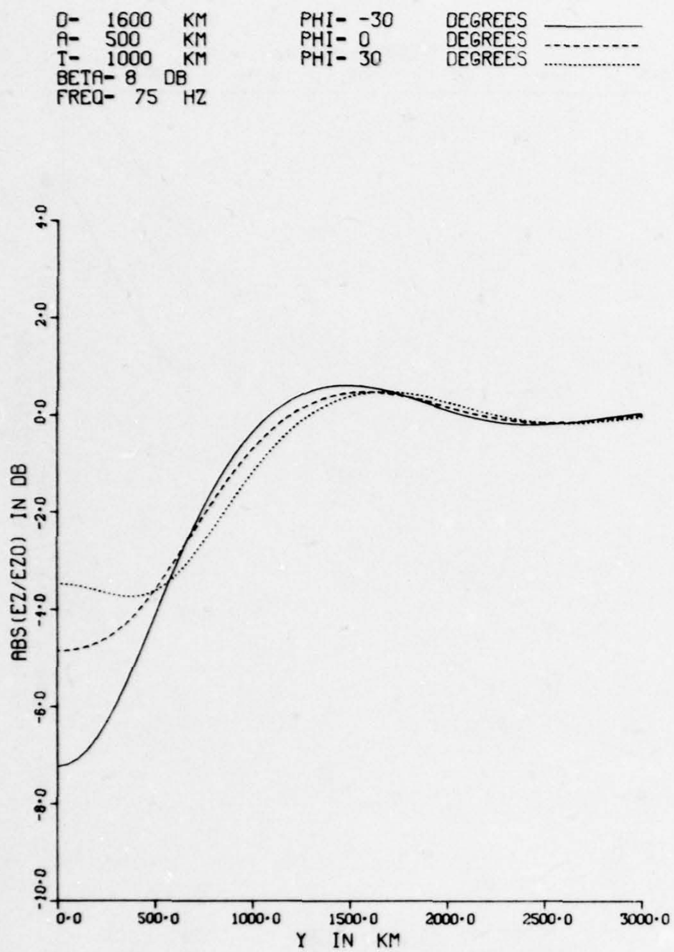

Figure 9. Signal level versus off path location (D = 1600 km, A = 500 km, T = 1,000 km, β = 8 dB, ϕ = -30°, 0°, 30°).

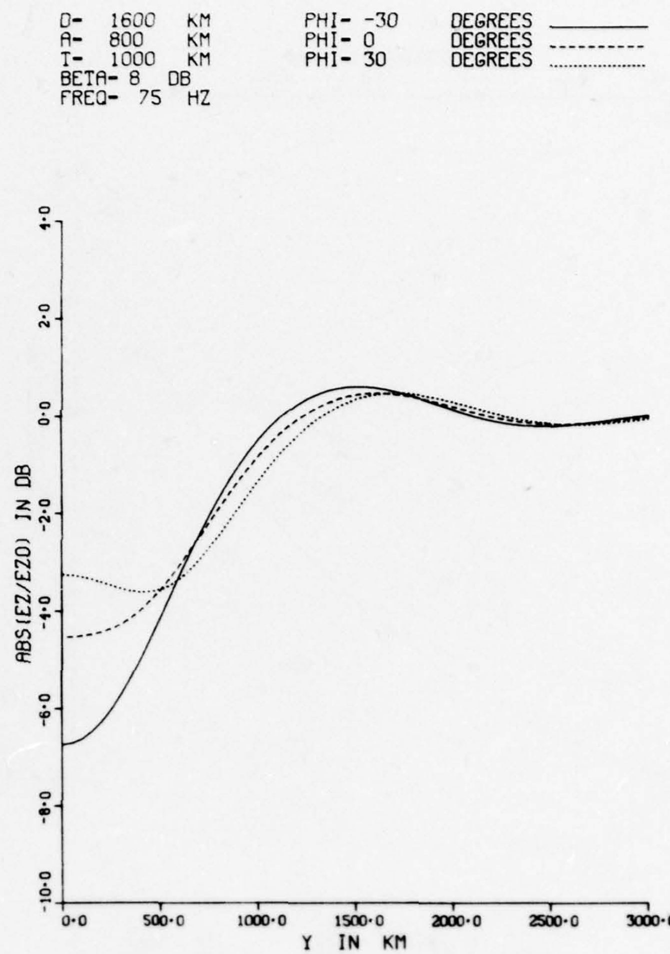

Figure 10. Signal level versus off path location (D = 1600 km, A = 800 km, T = 1,000 km, β = 8 dB, ϕ = -30°, 0°, 30°).

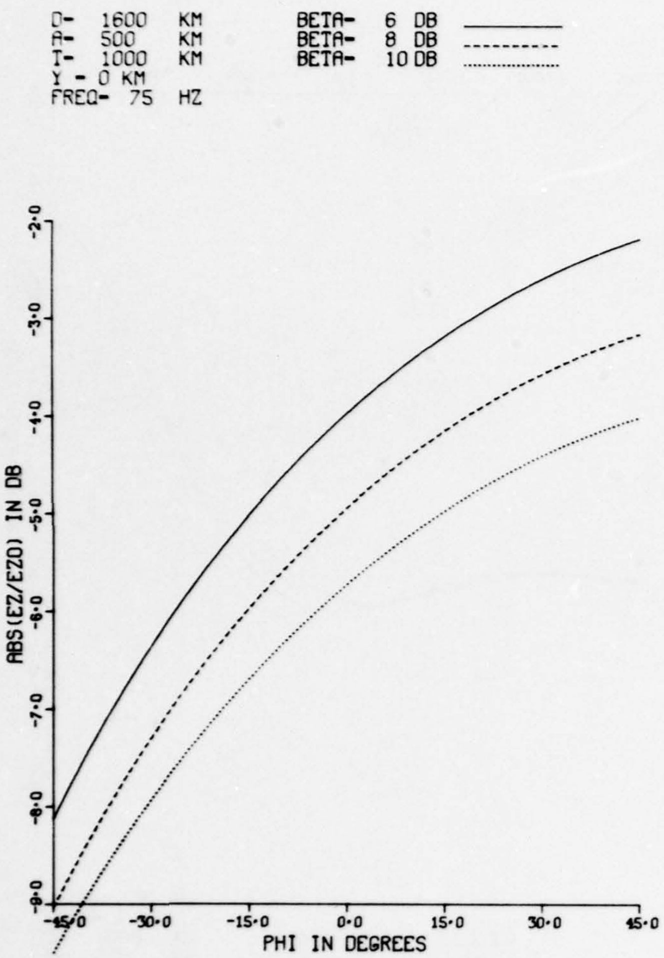

Figure 11. Signal level versus phi (D = 1600 km, A = 500 km, T = 1,000 km, β = 6, 8, 10 dB).

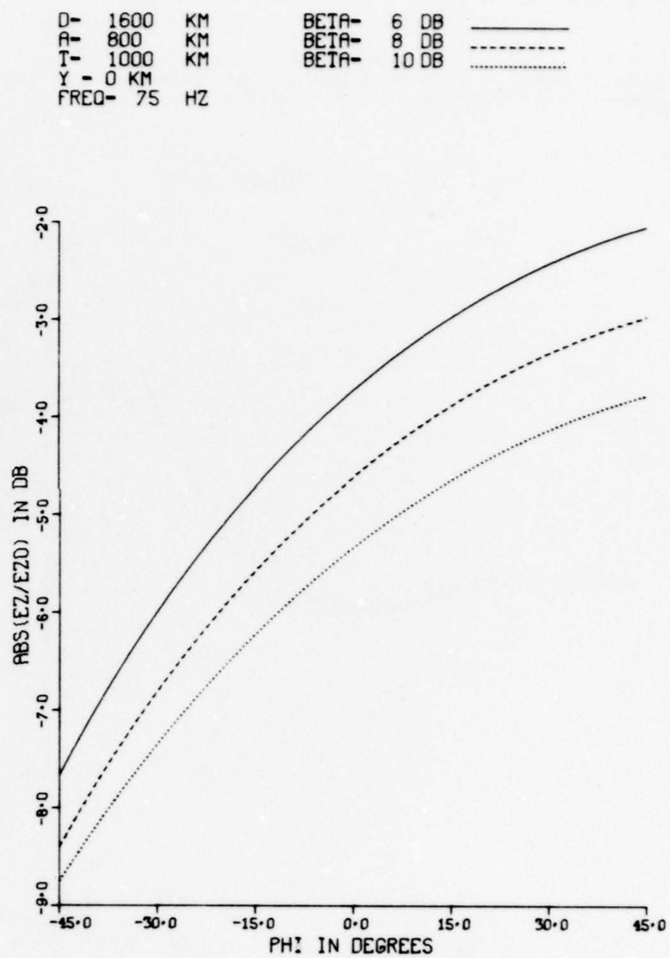

Figure 12. Signal level versus phi (D = 1600 km, A = 800 km, T = 1,000 km, β = 6, 8, 10 dB).

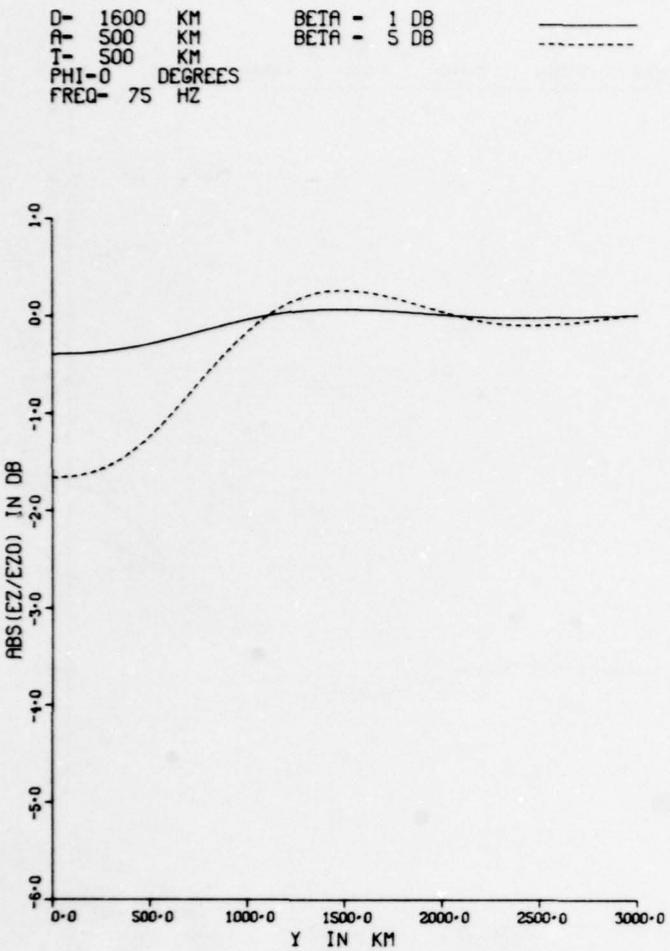

Figure 13. Signal level versus off path location (D = 1600 km, A = 500 km, T = 500 km, $\beta = 1, 5$ dB, $\phi = 0°$).

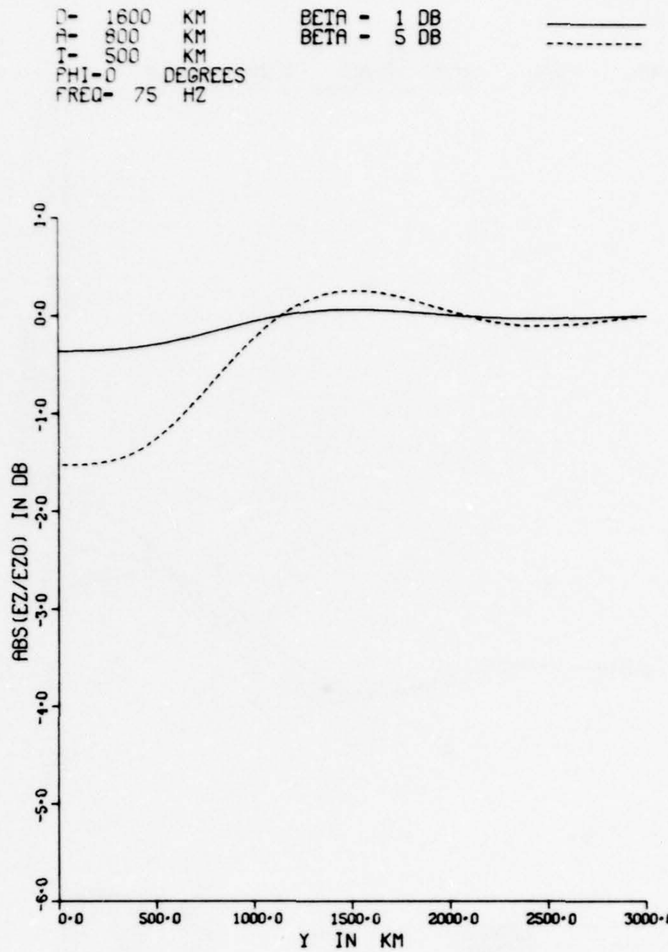

Figure 14. Signal level versus off path location (D = 1600 km, A = 800 km, T = 500 km, $\beta = 1, 5$ dB, $\phi = 0°$).

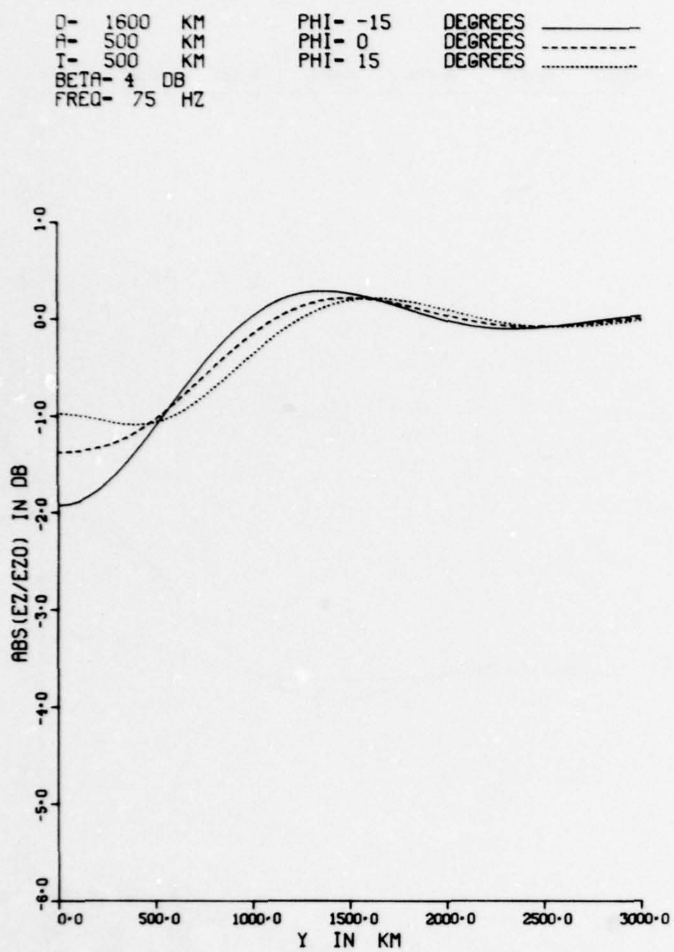

Figure 15. Signal level versus off path location (D = 1600 km, A = 500 km, T = 500 km, β = 4 dB, ϕ = -15°, 0°, 15°).

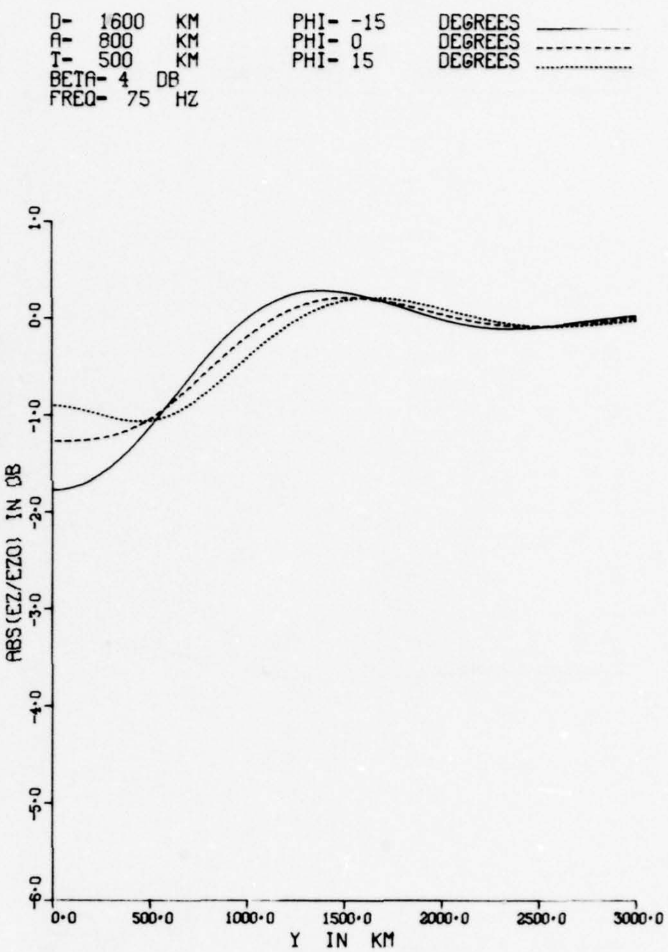

Figure 16. Signal level versus off path location (D = 1600 km, A = 800 km, T = 500 km, β = 4 dB, ϕ = -15°, 0°, 15°).

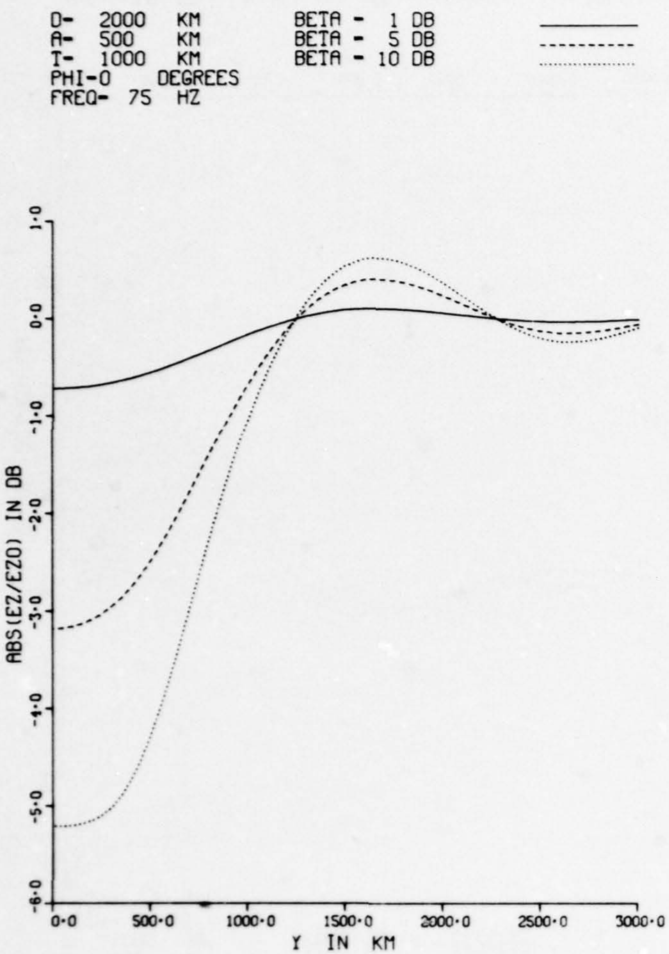

Figure 17. Signal level versus off path location (D = 2000 km, A = 500 km, T = 1,000 km, β = 1, 5, 10 dB, $\phi = 0°$).

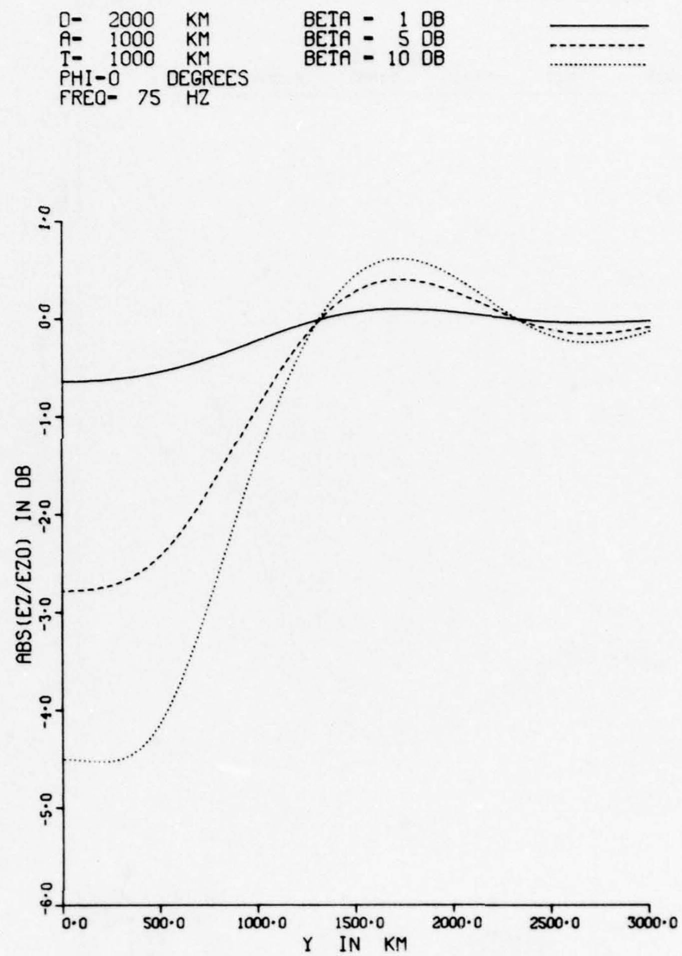

Figure 18. Signal level versus off path location (D = 2000 km, A = 1,000 km, T = 1000 km, β = 1, 5, 10 dB, $\phi = 0°$).

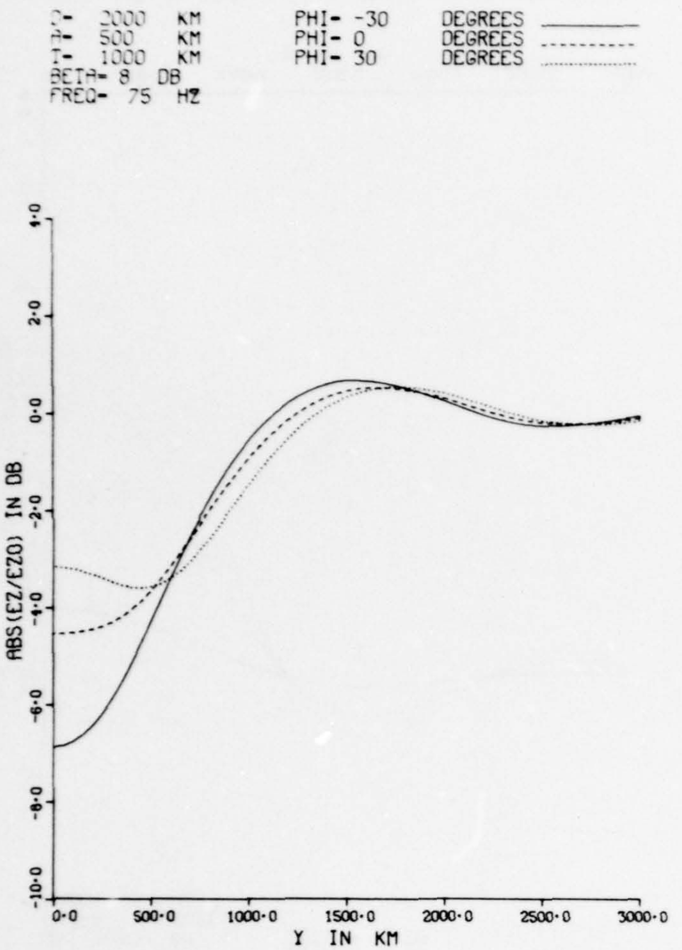

Figure 19. Signal level versus off path location (D = 2000 km, A = 500 km, T = 1,000 km, β = 8 dB, ϕ = -30°, 0°, 30°).

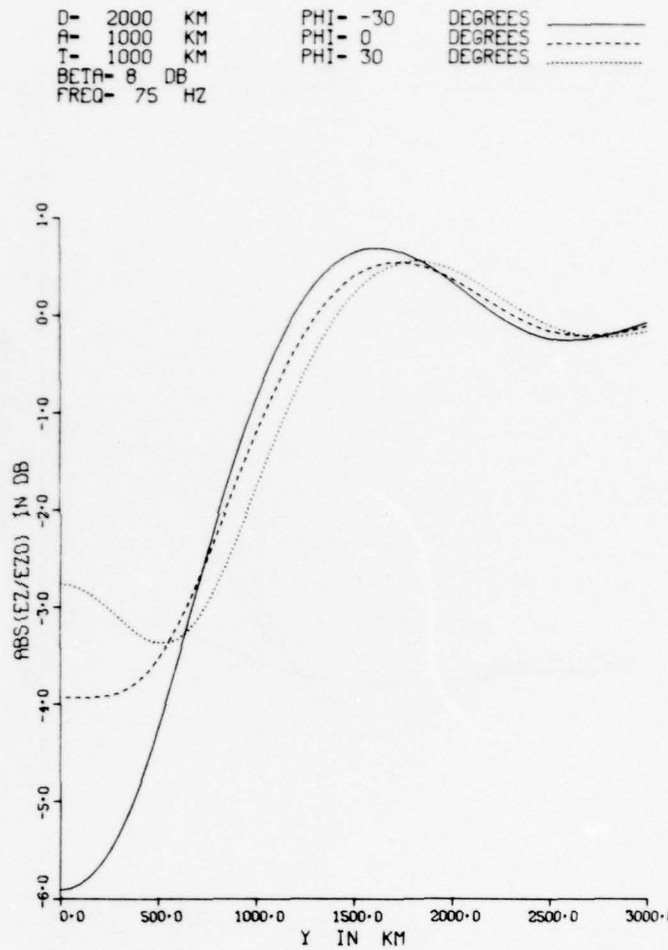

Figure 20. Signal level versus off path location (D = 2000 km, A = 1000 km, T = 1,000 km, β = 8 dB, ϕ = 30°, 0°, 30°).

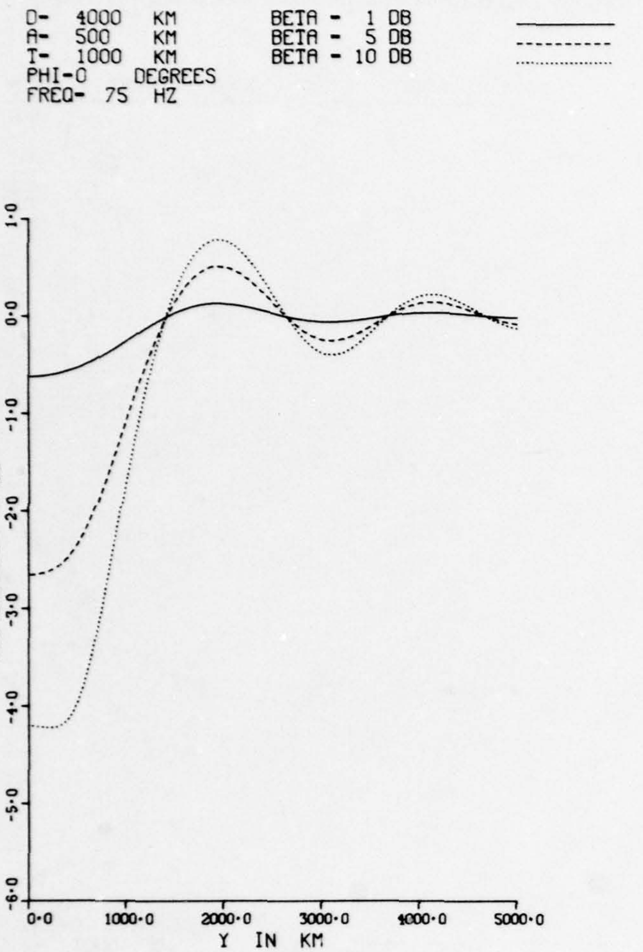

Figure 21. Signal level versus off path location (D = 4000 km, A = 500 km, T = 1000 km, β = 1, 5, 10 dB, ϕ = 0°).

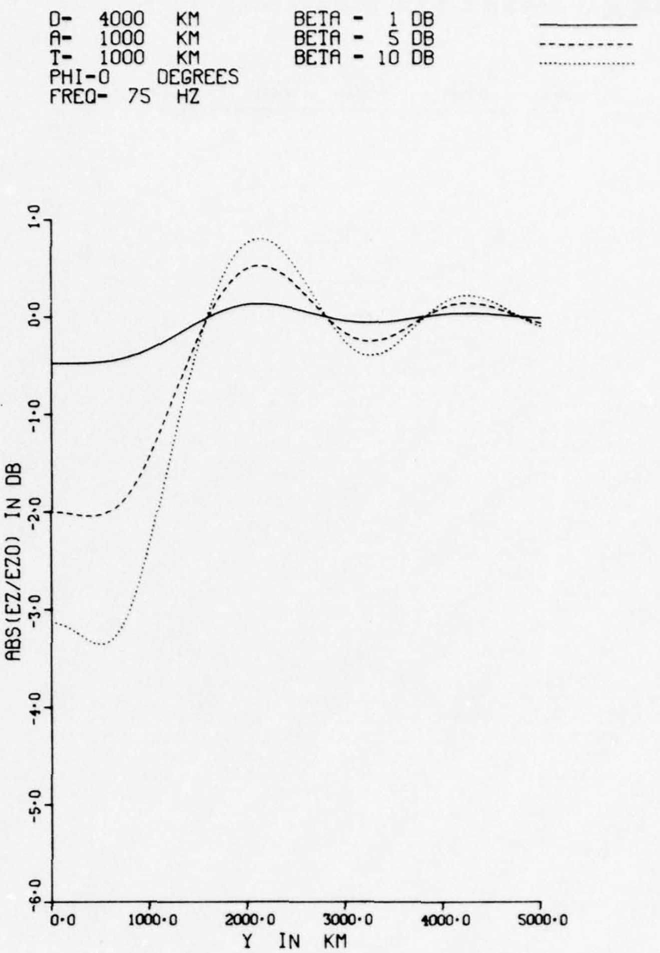

Figure 22. Signal level versus off path location (D = 4000 km, A = 1000 km, T = 1000 km, β = 1, 5, 10 dB, ϕ = 0°).

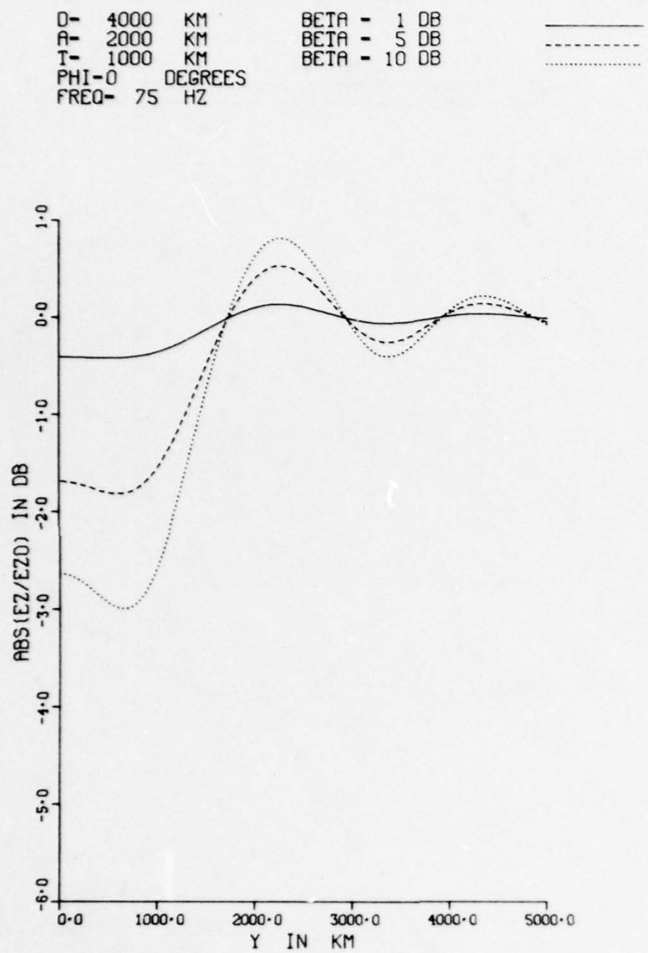

Figure 23. Signal level versus off path location (D = 4000 km, A = 2000 km, T = 1000 km, β = 1, 5, 10 dB, $\phi = 0^{\circ}$).

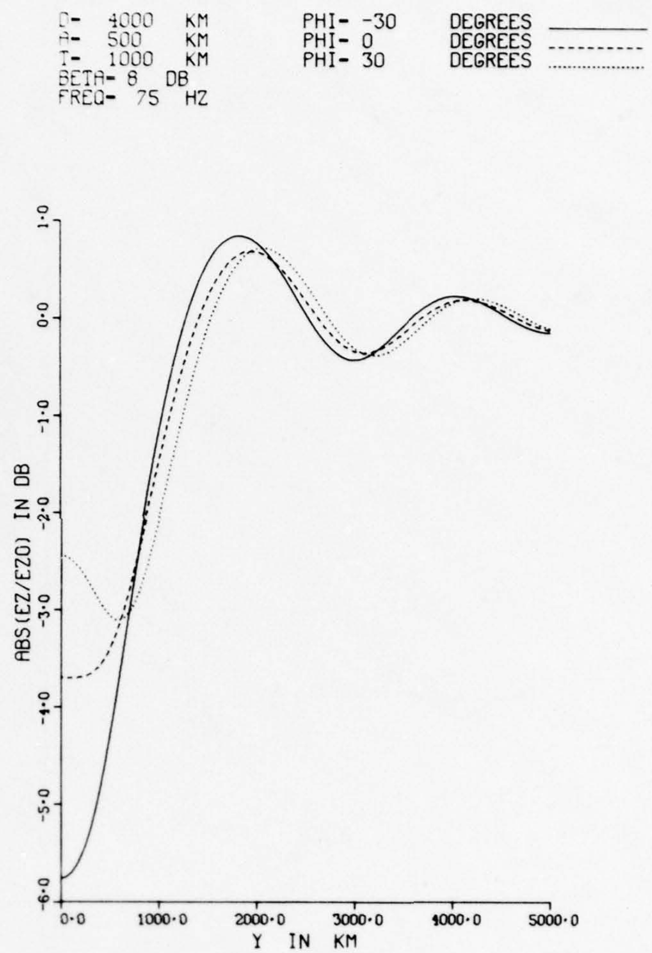

Figure 24. Signal level versus off path location (D = 4000 km, A = 500 km, T = 1000 km, β = 8 dB, $\phi = -30^{\circ}, 0^{\circ}, 30^{\circ}$).

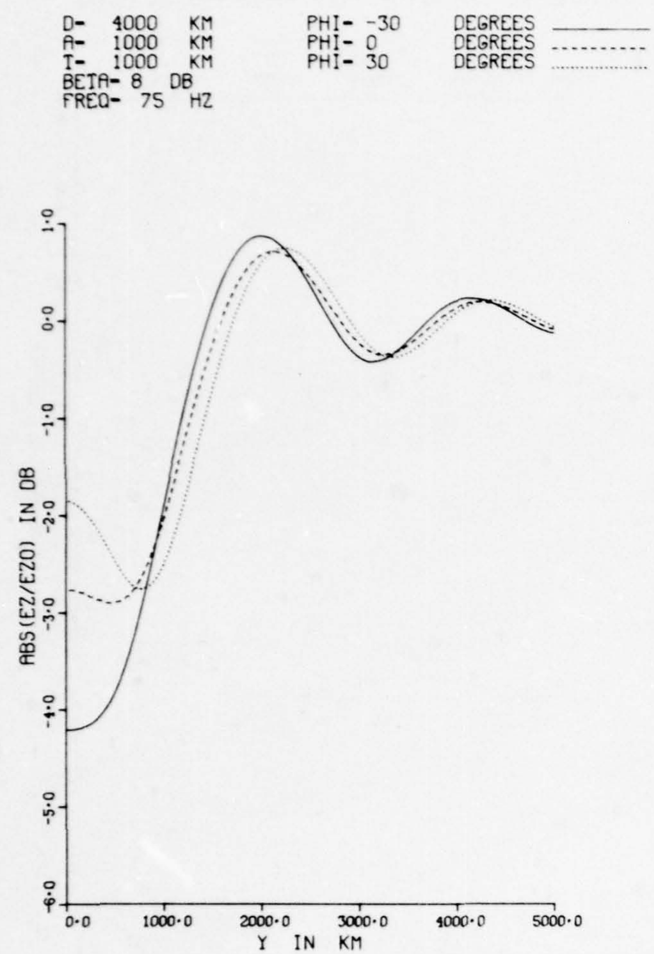

Figure 25. Signal level versus off path location (D = 4000 km, A = 1000 km, T = 1000 km, β = 8 dB, ϕ = -30°, 0°, 30°).

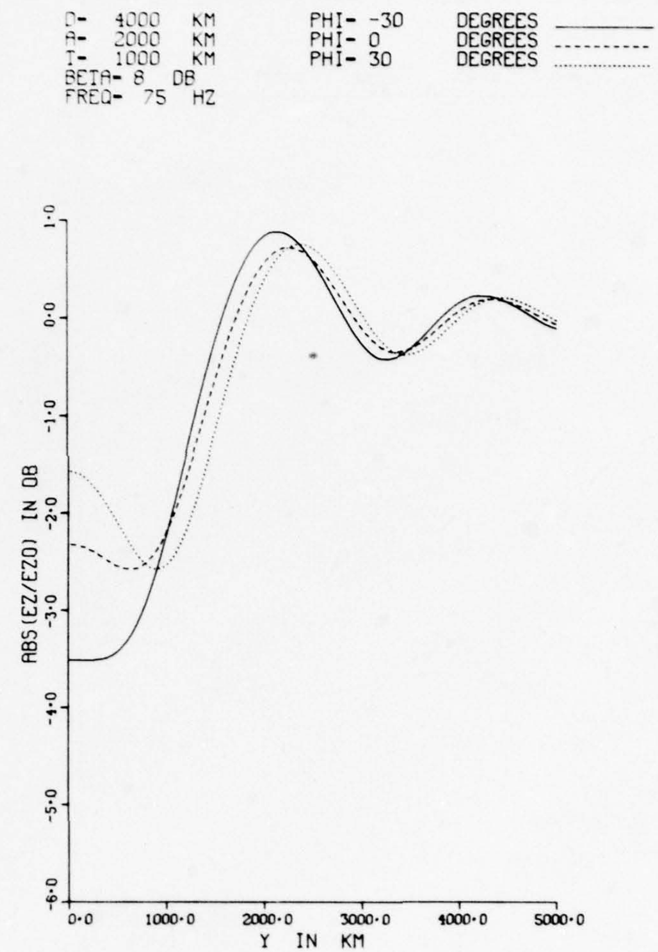

Figure 26. Signal level versus off path location (D = 4000 km, A = 2000 km, T = 1000 km, β = 8 dB, ϕ = -30°, 0°, 30°).

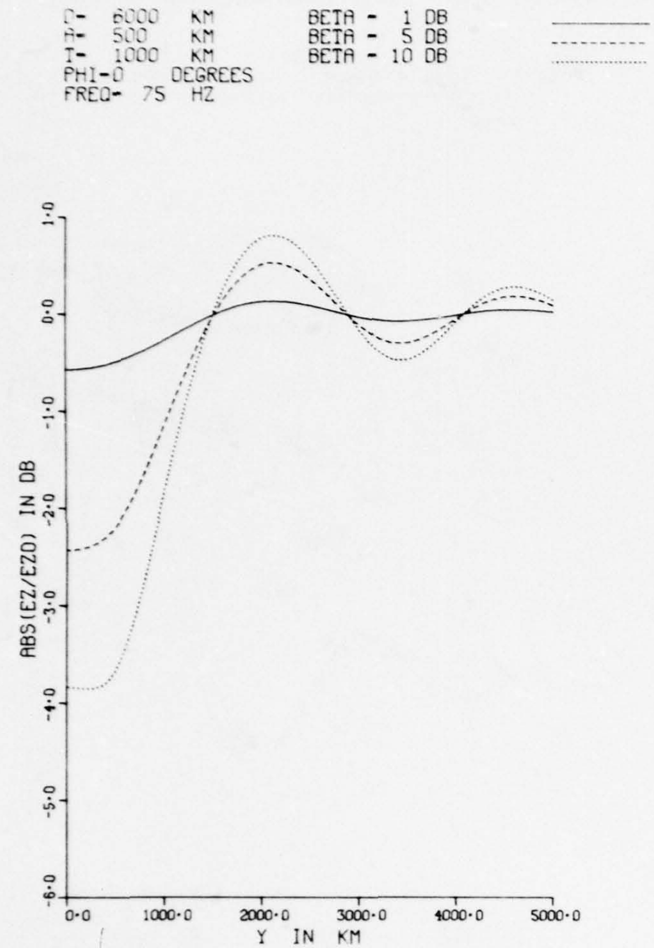

Figure 27. Signal level versus off path location (D = 6000 km, A = 500 km, T = 1000 km, β = 1, 5, 10 dB, $\phi = 0^{\circ}$).

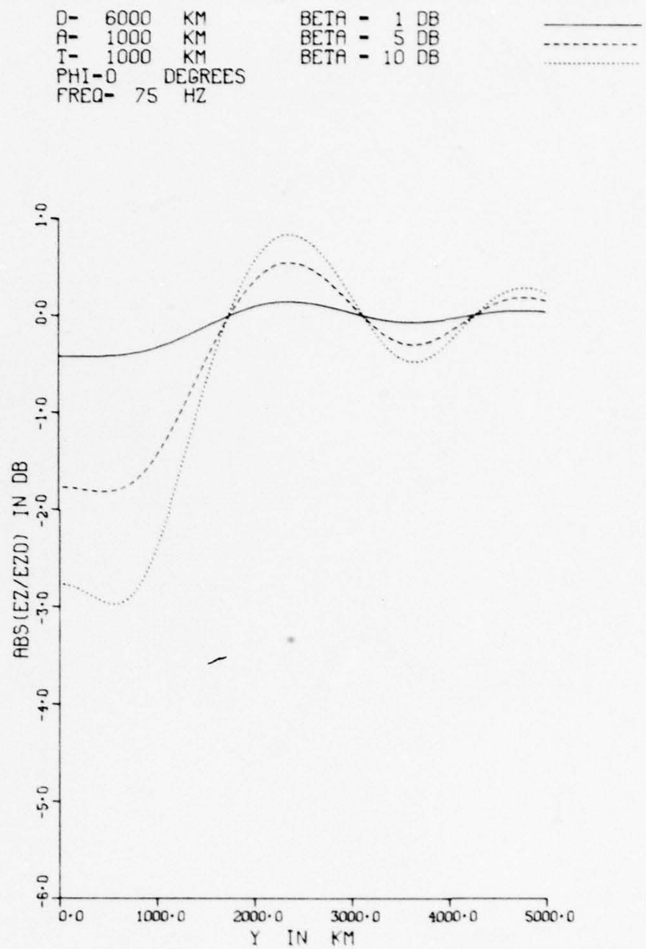

Figure 28. Signal level versus off path location (D = 6000 km, A = 1000 km, T = 1000 km, β = 1, 5, 10 dB, $\phi = 0^{\circ}$).

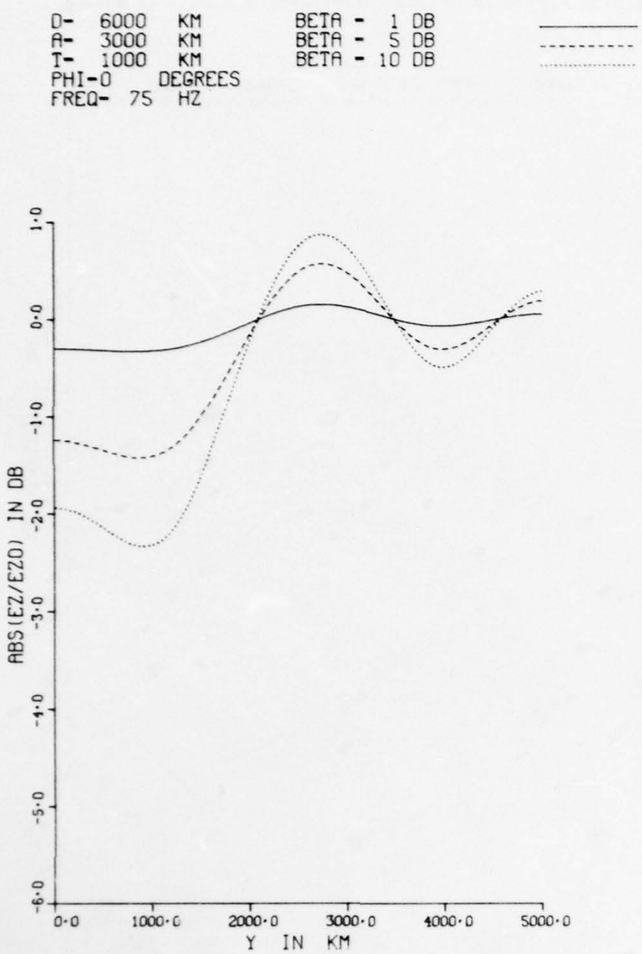

Figure 29. Signal level versus off path location (D = 6000 km, A = 3000 km, T = 1000 km, β = 1, 5, 10 dB, ϕ = 0°).

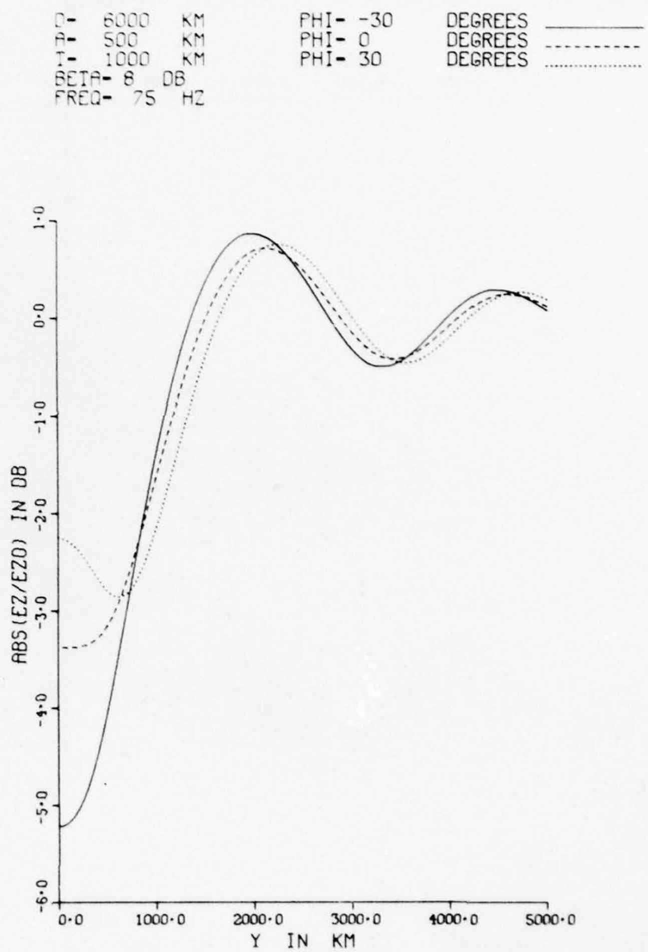

Figure 30. Signal level versus off path location (D = 6000 km, A = 500 km, T = 1000 km, β = 8 dB, ϕ = -30°, 0°, 30°).

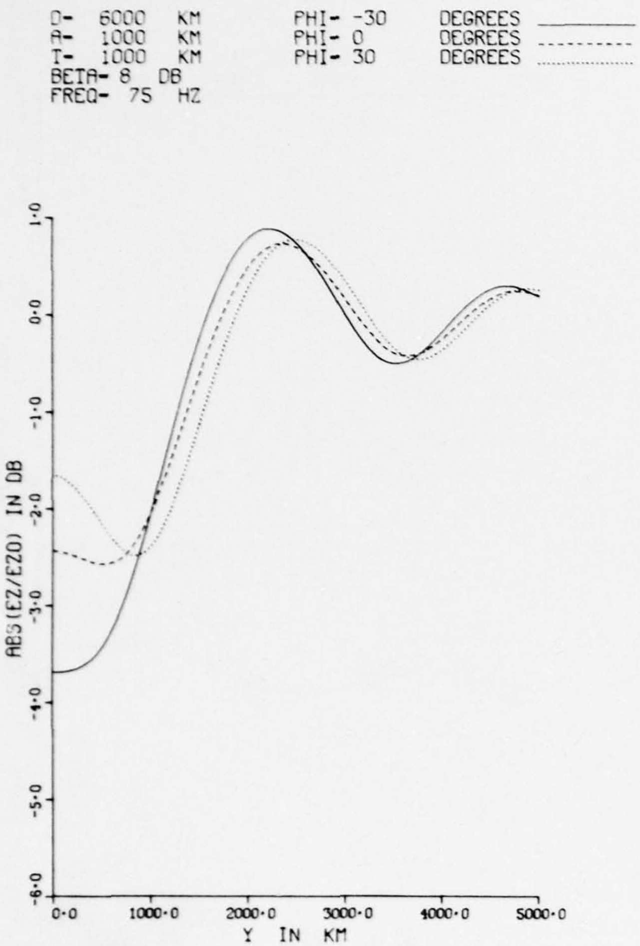

Figure 31. Signal level versus off path location (D = 6000 km, A = 1000 km, T = 1000 km, β = 8 dB, ϕ = -30°, 0°, 30°).

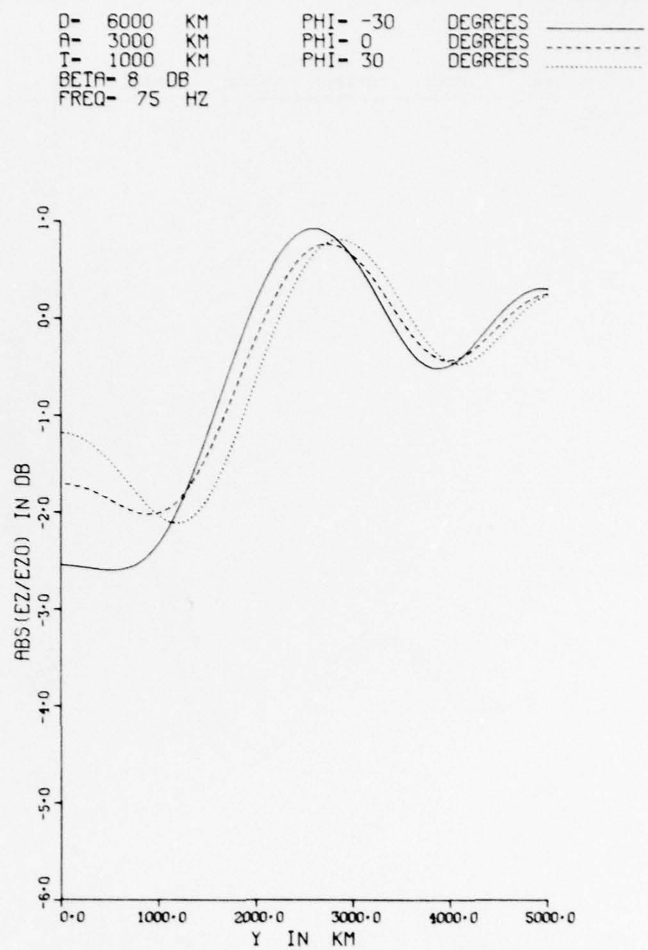

Figure 32. Signal level versus off path location (D = 6000 km, A = 3000 km, T = 1000 km, β = 8 dB, ϕ = -30°, 0°, 30°).

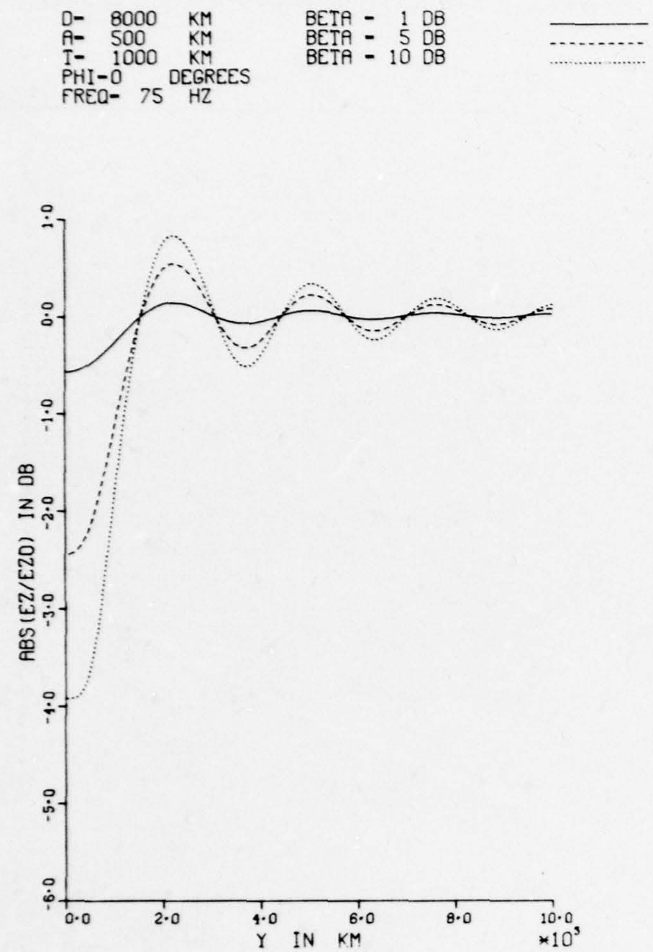

Figure 33. Signal level versus off path location (D = 8000 km, A = 500 km, T = 1000 km, β = 1, 5, 10 dB, ϕ = 0°).

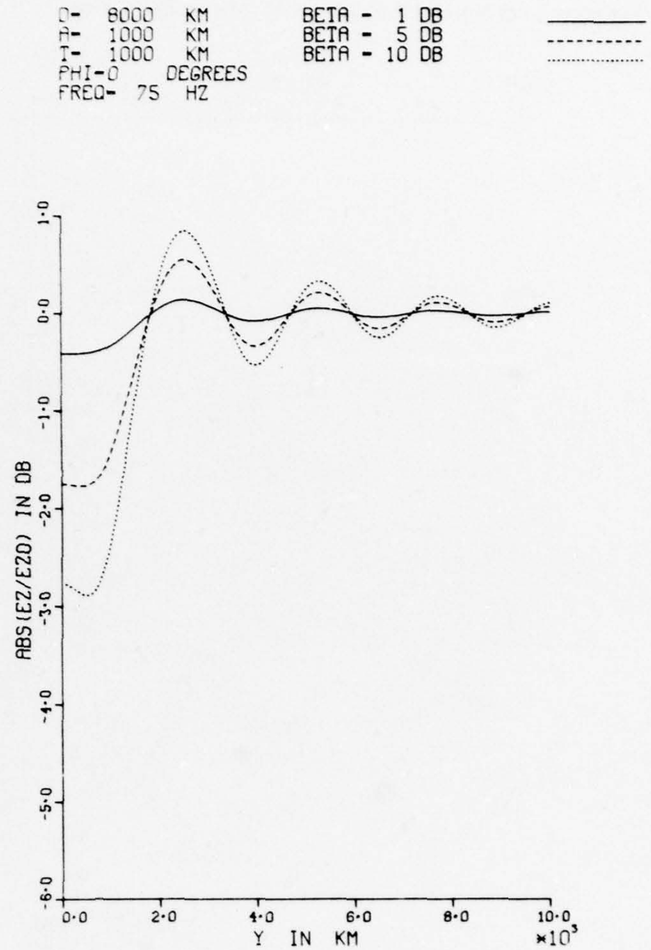

Figure 34. Signal level versus off path location (D = 8000 km, A = 1000 km, T = 1000 km, β = 1, 5, 10 dB, ϕ = 0°).

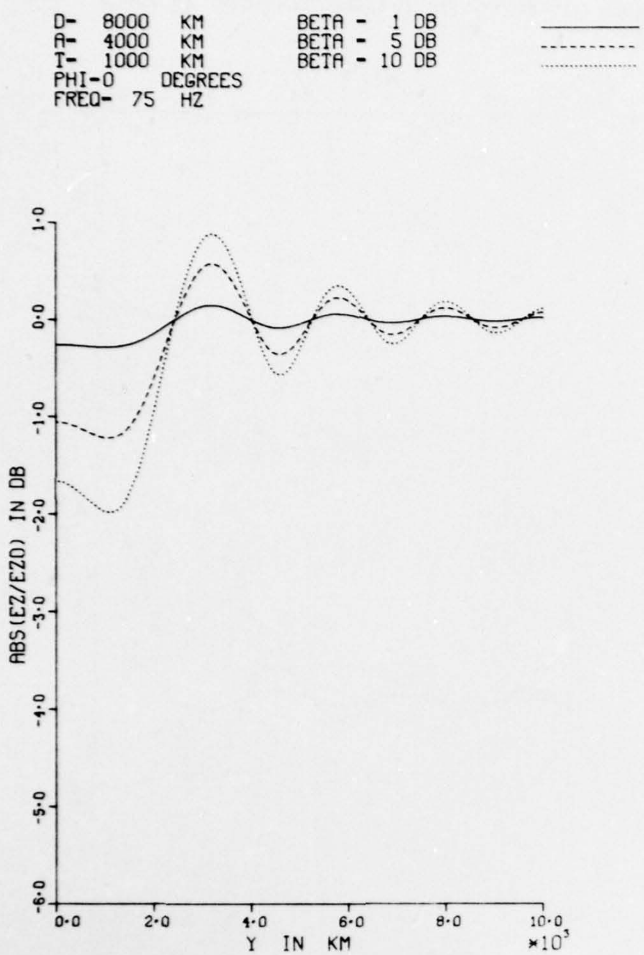

Figure 35. Signal level versus off path location (D = 8000 km, A = 4000 km, T = 1000 km, β = 1, 5, 10 dB, $\phi = 0°$).

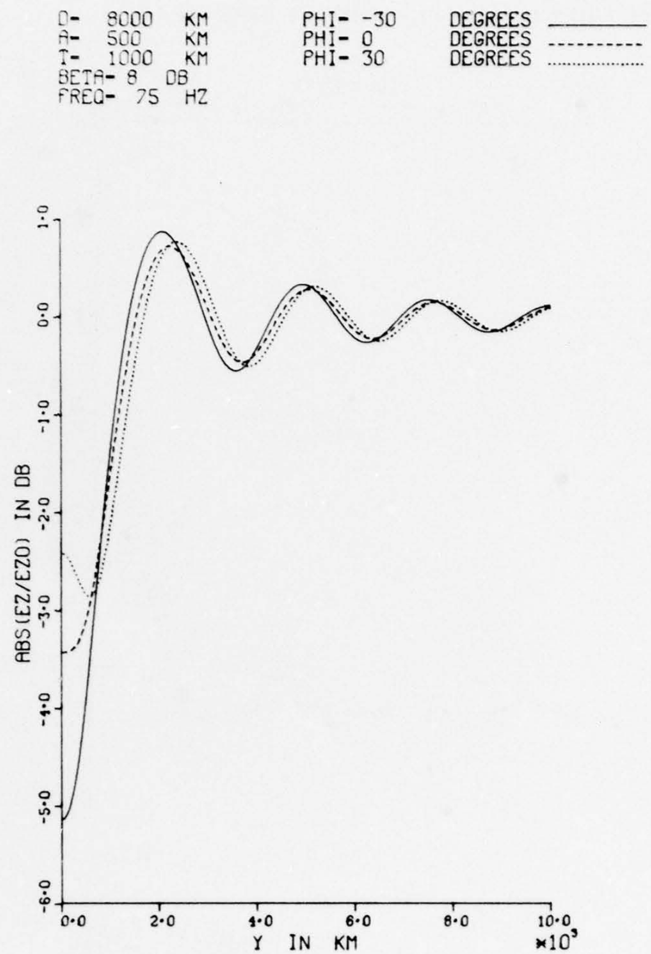

Figure 36. Signal level versus off path location (D = 8000 km, A = 500 km, T = 1000 km, β = 8 dB, $\phi = -30°, 0°, 30°$).

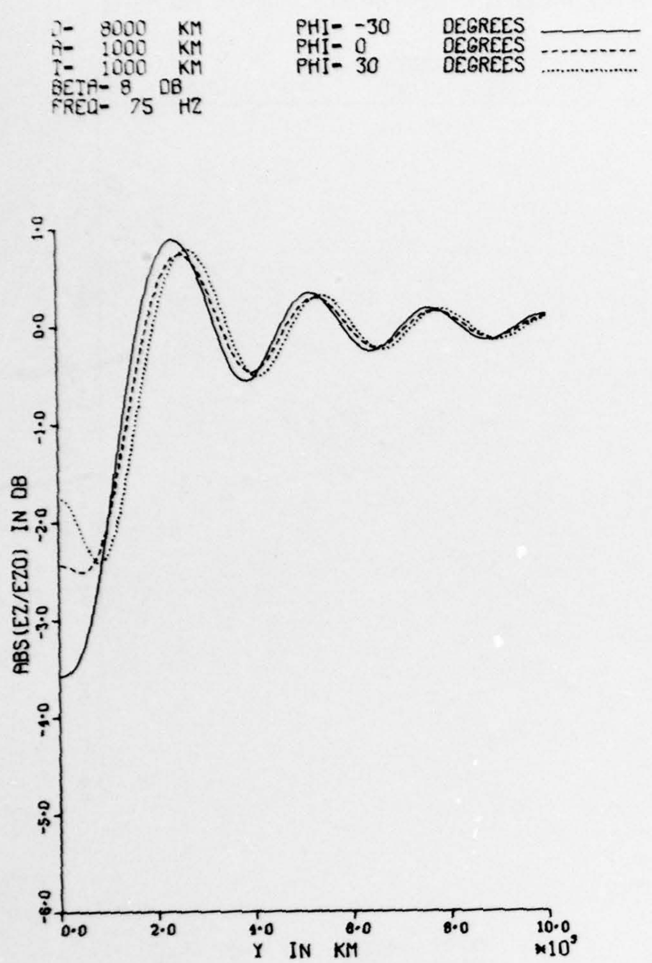

Figure 37. Signal level versus off path location (D = 8000 km, A = 1000 km, T = 1000 km, β = 8 dB, ϕ = -30°, 0°, 30°).

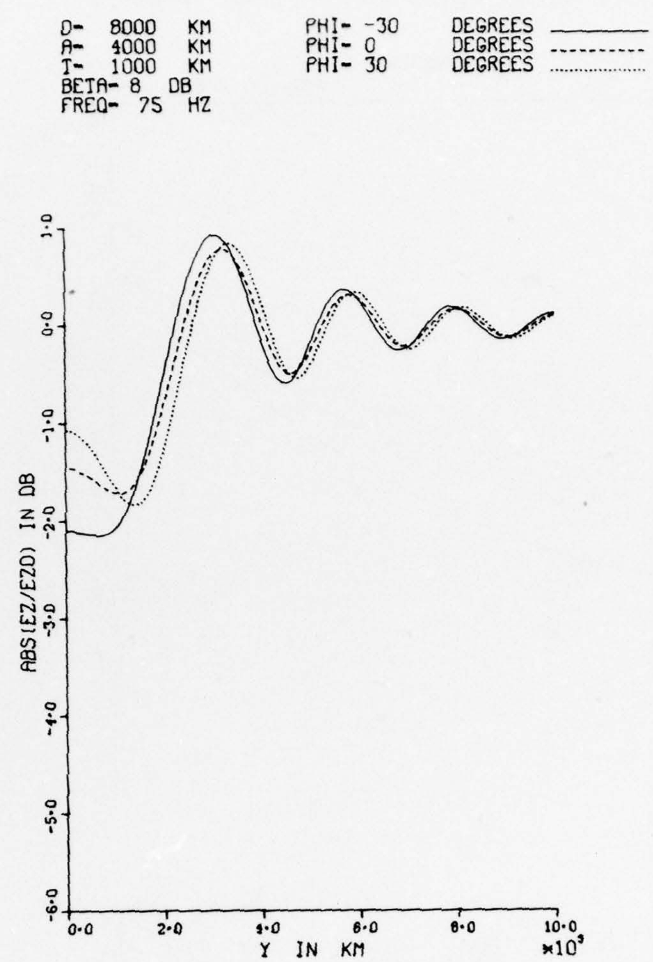

Figure 38. Signal level versus off path location (D = 8000 km, A = 4000 km, T = 1000 km, β = 8 dB, ϕ = -30°, 0°, 30°).

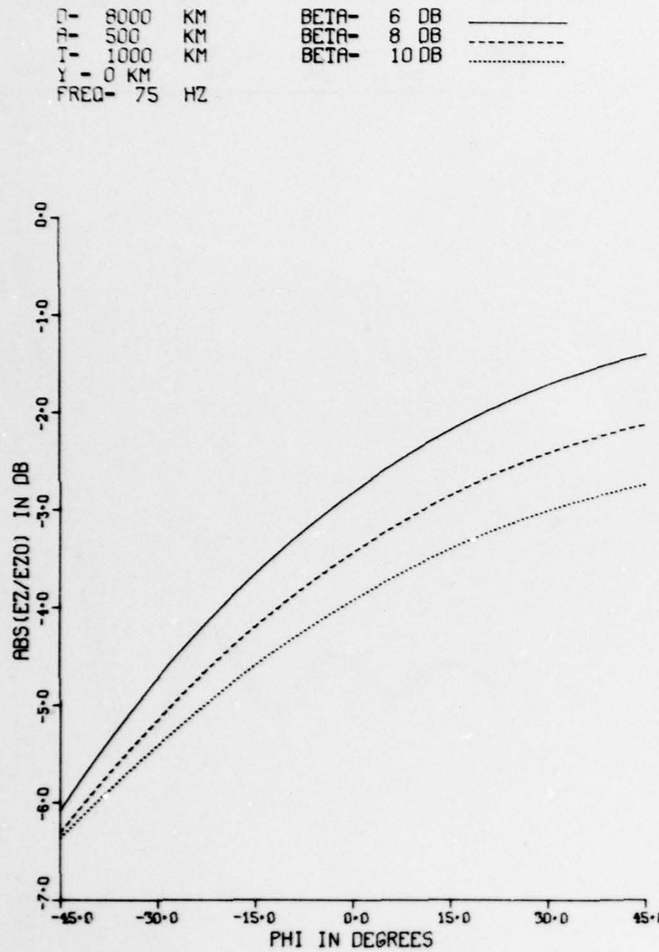

Figure 39. Signal level versus phi (D = 8000 km, A = 500 km, T = 1000 km, β = 6, 8, 10 dB).

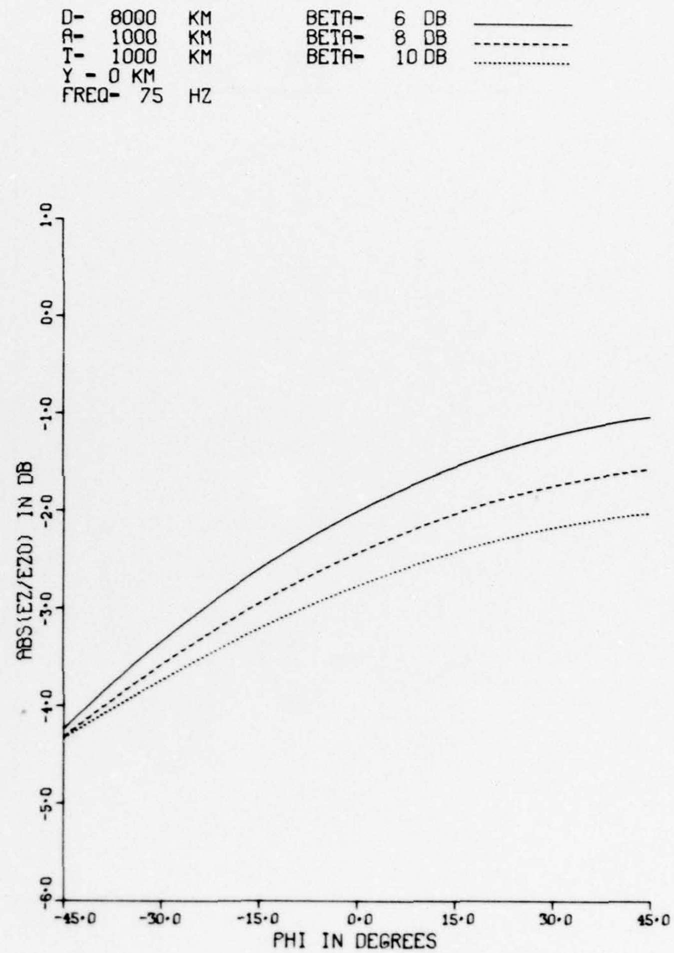

Figure 40. Signal level versus phi (D = 8000 km, A = 1000 km, T = 1000 km, β = 6, 8, 10 dB).

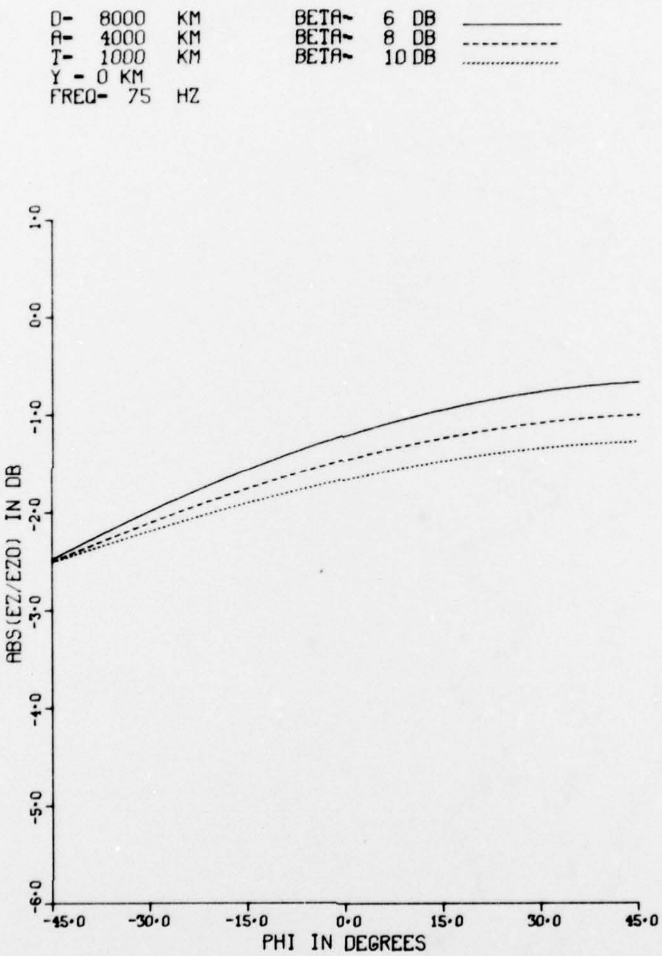

Figure 41. Signal level versus phi (D = 8000 km, A = 4000 km, T = 1000 km, β = 6, 8, 10 dB).

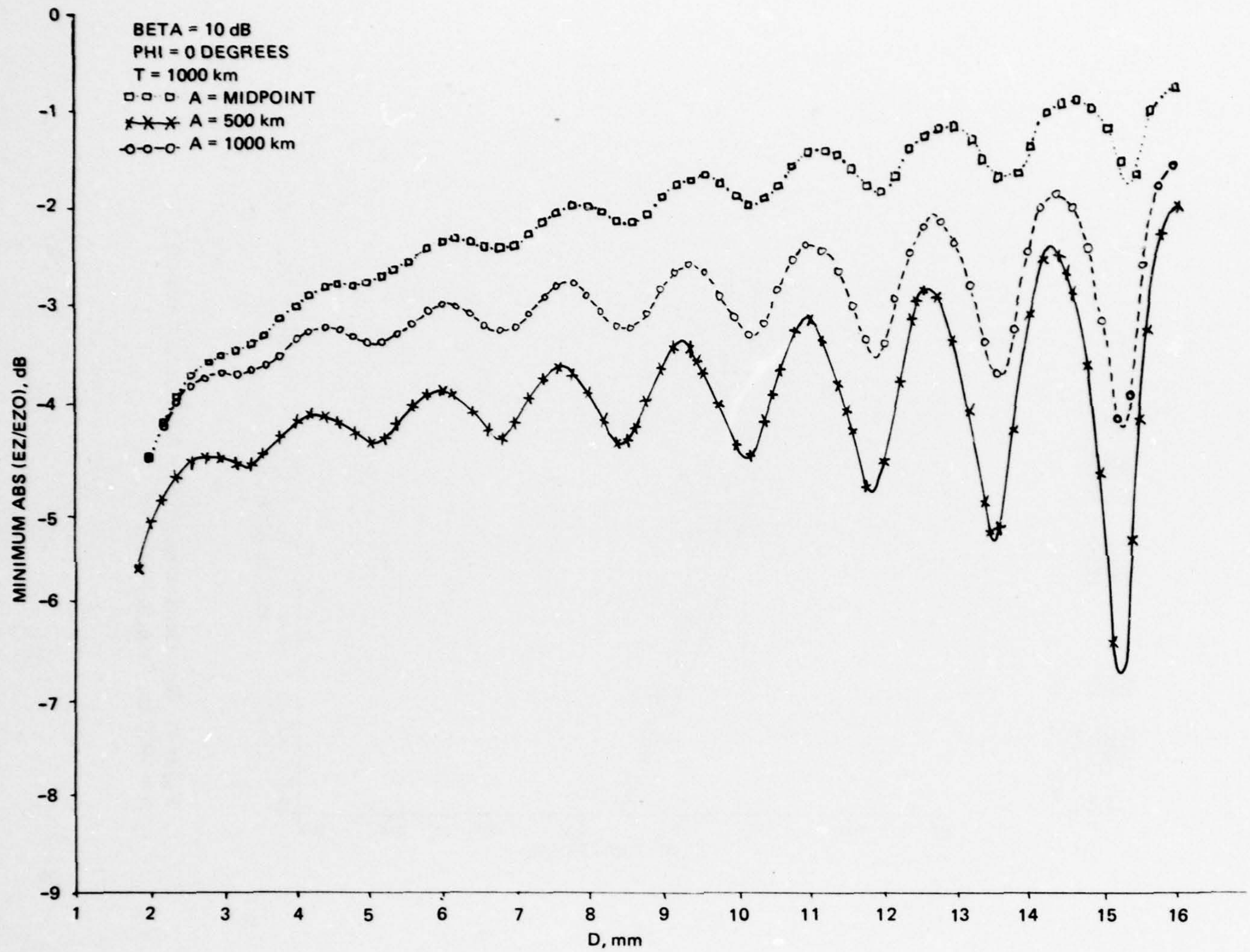

Figure 42. Minimum signal level versus transmitter-receiver distance.

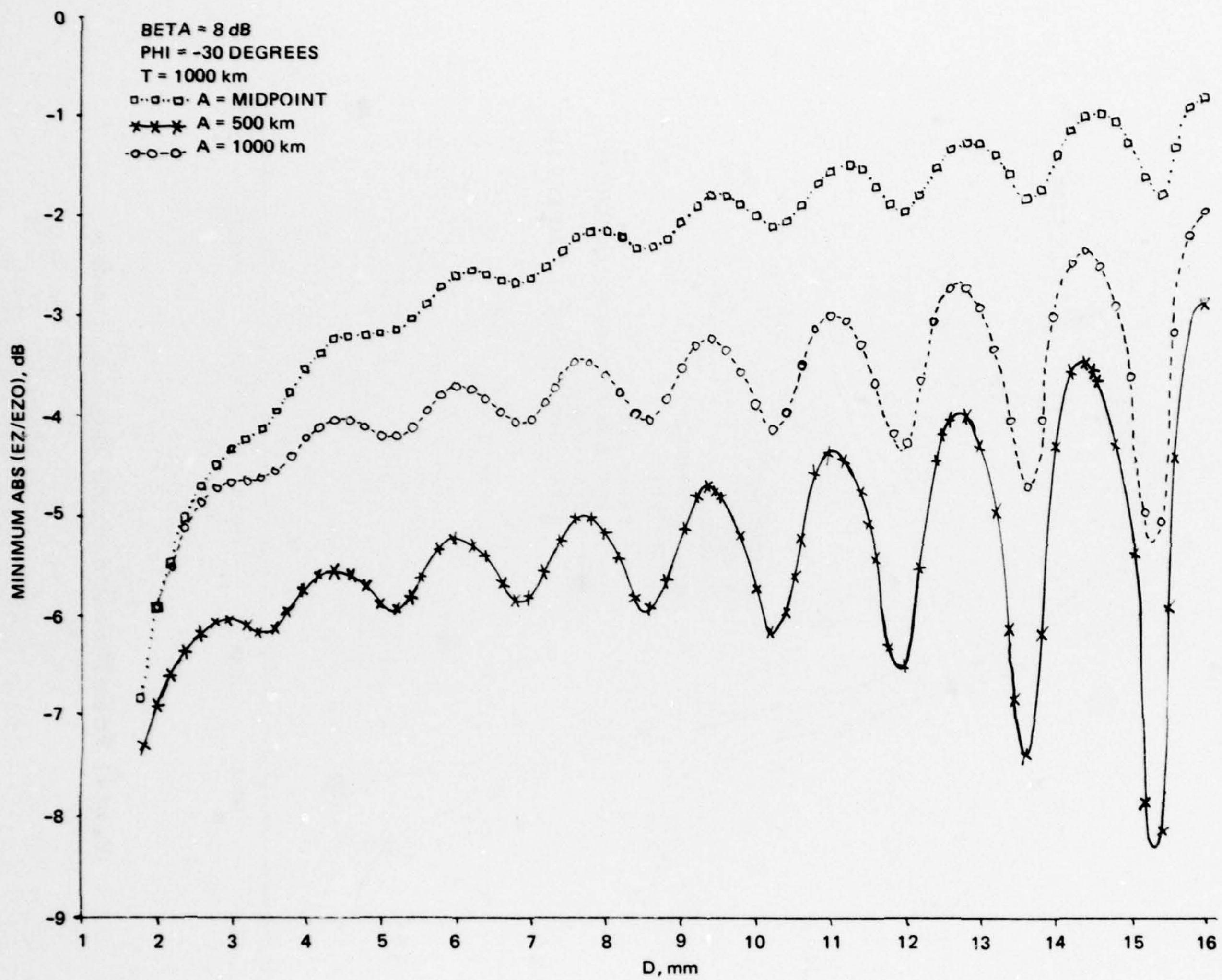

Figure 43. Minimum signal level versus transmitter-receiver distance.

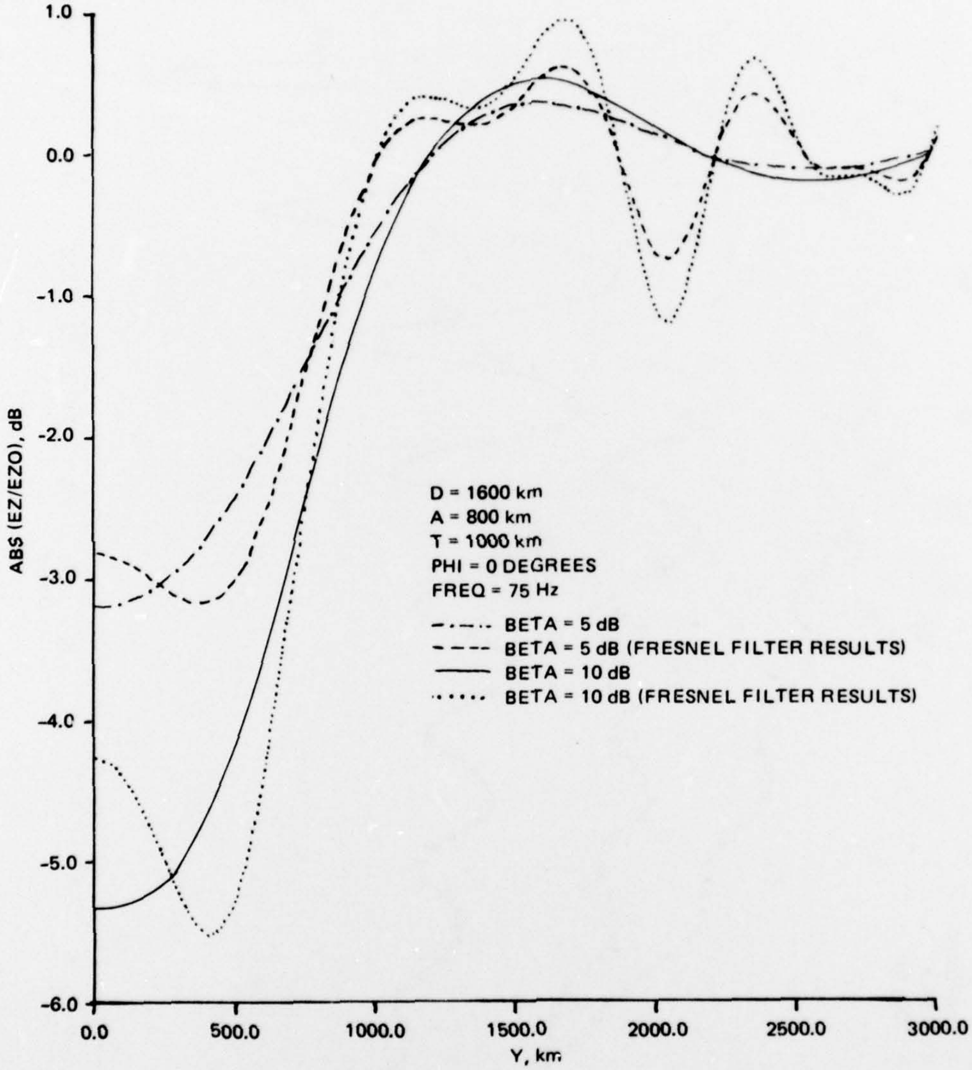

Figure 44. Fresnel filtering and numerical integration comparisons.

IV. CONCLUSIONS

A simple Kirchhoff-Huygens diffraction model has been used to estimate the effect of a finite sized patch of sporadic E on lower ELF propagation. The patch is approximated by a lumped parameter phase-amplitude screen allowed to move along a great circle path transverse to the transmitter-receiver great circle path.

The results indicate that sporadic E patches on the order of 1000 km × 1000 km causing phase rate shifts, and attenuation rate enhancements consistent with full wave modal evaluations, can account for the 6–8 dB fades observed in connection with the 1600 km WTF transmissions. The results suggest also that such disturbances can be expected to produce 2 to 4 dB fades over paths as long as 10,000 km. Deep fades require the center of the phase amplitude screen to be well within the first Fresnel zone and the effects of the disturbances are highly damped out when the center of the phase-amplitude screen exceeds about two Fresnel zones. It has been shown that phase shifts as well as attenuation enhancement can be influential in determining the perturbed signal. In fact, the deepest fades encountered in the present study were with the combination $\phi = -30°$, $\beta = 8$ dB.

No allowance for excitation factor effects has been made in the study even though Figures 5 and 6 indicate that such effects could be important should the disturbed region fall over either the transmitter or receiver. Such effects would be best handled by a full wave treatment of the problem and the calculations presented in this study fully support the need for such programs. Development of the latter would benefit from a concurrent measurement program simultaneously involving nocturnal ELF propagation and sporadic E soundings over and about the path.

BIBLIOGRAPHY

Bannister, P. R., "Variations in extremely low frequency propagation parameters," J. Atmos. Terr. Phys. 37, pp. 1203–1210, 1975.

Barr, R., "The effect of sporadic-E on the nocturnal propagation of ELF radio waves," J. Atmos. Terr. Phys., 39, pp. 1379–1387, 1977.

Crombie, D. D., "The effects of a small local change in phase velocity on the propagation of a vlf radio signal," NBS Report 7998, Dec. 1963, pp. 28.

Davis, J. R., "Localized nighttime D-region disturbances and ELF propagation," J. Atmos. Terr. Phys. 38, pp. 1309–1317, 1976.

Davis, J. R. & Meyers, W. D., "Observations of ELF signal and noise variability on northern latitude paths," NRL Report 7923, Nov. 1975, pp. 17.

Galejs, J., "ELF propagation in an inhomogeneous waveguide," Radio Science 6(7), pp. 727–736, 1971.

Griefinger, C. & Griefinger, P., "Effect of a cylindrically-symmetric ionospheric disturbance on ELF propagation in the earth ionosphere waveguide," DNA 4339T prepared for the Defense Nuclear Agency by R&D associates, 1977, pp. 40.

Marcuse, D., "Light transmission optics," Van Nostrand Reinhold Co., New York, 1972.

Pappert, R. A. & Moler, W. F., "A theoretical study of ELF normal mode reflection and absorption produced by nighttime ionospheres," to be published in J. Atmos. Terr. Phys.

Pappert, R. A. & Shockey, L. R., "Ionospheric reflection and absorption properties of normal modes at ELF." Interim Report No. 772, prepared for the Defense Nuclear Agency by the Naval Ocean Systems Center, Sept. 1977, pp. 102.

Shellman, C., "A proposed formulation for describing the propagation of ELF fields in the spherical earth-ionosphere waveguide." Naval Ocean Systems Center Tech. Note 208, 1977, pp. 37.

Wait, J. R., "Calculated diffraction effects at VLF from a localized ionospheric depression." NBS Tech Note No. 208, Jan. 1964a, pp. 12.

Wait, J. R., "On phase changes in very-low-frequency propagation induced by ionospheric depression of finite extent." J. Geophy. Res., 69(3), pp. 441–445, 1964b.

Whitehead, J. D., "Production and Prediction of Sporadic E." Rev. of Geophys. and Space Physics," 8(1), pp. 65–144, 1970.

Wilcox, T. J., "Scattering of ELF waves by localized ionospheric perturbations." TRW Systems Group Internal Report TRW 4360.7.74-50, March 1974, pp. 21.

INITIAL DISTRIBUTION LIST

Department of Defense

Assistant Secretary of Defense
CMD, CONT, COMM & INTELL
Department of Defense
Washington, DC 20301
01CY ATTN M. Epstein
01CY ATTN J. Babcock

Director
Command Control Technical Center
Pentagon Rm BE 685
Washington, DC 20301
01CY ATTN C-650
01CY ATTN C-312

Director
Defense Advanced Research Project Agency
Architect Building
1400 Wilson Blvd.
Arlington, VA 22209
01CY ATTN Nuclear Monitoring Rsch
01CY ATTN Strategic Tech. Office

Defense Communication Engineering Center
1860 Wiehle Avenue
Reston, VA 22090
01CY ATTN Code R220 M. Horowitz
01CY ATTN Code R720 John Worthington
01CY Code R410 James W. McLean
01CY Code R103

Director
Defense Communications Agency
Washington, DC 20305
01CY ATTN Code 810 R. W. Rostron
01CY ATTN Code 480
01CY ATTN Code 101B MAJ Rood

Defense Communications Agency
WWMCCS System Engineering Org
Washington, DC 20305
01CY ATTN R. L. Crawford

Defense Documentation Center
Cameron Station
Alexandria, VA 22314
12CY ATTN TC

Director
Defense Intelligence Agency
Washington, DC 20301
01CY ATTN DIAST-5
01CY ATTN DIAAP Albert L. Wise
01CY ATTN DB-4C Edward OFarrell

Director
Defense Nuclear Agency
Washington, DC 20305
01CY ATTN DDST
01CY ATTN TISI Archives
03CY ATTN TITL Tech. Library
03CY ATTN RAAE
01CY ATTN STVL

Commander
Field Command
Defense Nuclear Agency
Kirtland AFB, NM 87115
01CY ATTN FCPR

Director
Interservice Nuclear Weapons School
Kirtland AFB, NM 87115
01CY ATTN Document Control

Director
Joint Strat TGT Planning Staff JCS
Offutt AFB
Omaha, NB 68113
01CY ATTN JPST CAPT D. G. Goetz

Chief
Livermore Division Fld Command DNA
Lawrence Livermore Laboratory
P.O. Box 808
Livermore, CA 94550
01CY ATTN FCPRL

Director
National Security Agency
FT. George G. Meade, MD 20755
01CY ATTN W65
01CY ATTN Oliver H. Bartlett W32
01CY ATTN Technical Library
01CY ATTN John Skillman R52

OJCS/J-3
The Pentagon
Washington, DC 20301
(Operations)
01CY ATTN WWMCCS Eval OFC Mr. Toma

OJCS/J-5
The Pentagon
Washington, DC 20301
(Plans & Policy)
01CY ATTN Nuclear Division

Under Secry of Defense for Research and Engineering
Department of Defense
Washington, DC 20301
01CY ATTN S&SS (OS)

Department of the Army

Commander/Director
Atmospheric Sciences Laboratory
US Army Electronics Command
White Sands Missile Range, NM 88002
01CY ATTN DELAS-AE-M F. E. Niles

Commander
Harry Diamond Laboratories
2800 Powder Mill Rd.
Adelphi, MD 20783
01CY ATTN DELHD-NP Francis N. Wimenitz
01CY ATTN Mildred H. Weiner DRXDO-II

Commander
US Army Electronics Command
Fort Monmouth, NJ 07703
01CY ATTN DRSEL-RD
01CY ATTN J. E. Quigley

Commander
US Army Foreign Science & Tech. Center
220 7th Street, NE
Charlottesville, VA 22901
01CY ATTN R. Jones
01CY ATTN P. A. Crowley

Commander
US Army Nuclear Agency
7500 Backlick Road
Building 2073
Springfield, VA 22150
01CY ATTN MONA-WE J. Berberet

Chief
US Army Research Office
P.O. Box 12211
Triangle Park, NC 27709
01CY ATTN DRXRD-ZC

Department of the Navy

Chief of Naval Operations
Navy Department
Washington, DC 20350
01CY ATTN OP 941
01CY ATTN Code 604C3
01CY ATTN OP 943 LCDR Huff
01CY ATTN OP 981

Chief of Naval Research
Navy Department
Arlington, VA 22217
01CY ATTN Code 402
01CY ATTN Code 420
01CY ATTN Code 421
01CY ATTN Code 461
01CY ATTN Code 464

Commanding Officer
Naval Intelligence Support Center
4301 Suitland Rd. Bldg. 5
Washington, DC 20390
01CY ATTN Code 5404 J. Galet

Commander
Naval Ocean Systems Center
San Diego, CA 92152
01CY ATTN Code 81 H.D. Smith
03CY ATTN Code 532
01CY ATTN Code 532 William F. Moler

Director
Naval Research Laboratory
Washington, DC 20375
01CY ATTN Code 5410 John Davis
01CY ATTN Code 7701 Jack D. Brown
01CY ATTN Code 5461 Trans. Iono. Prop.
01CY ATTN Code 5465 Prop. Applications
01CY ATTN Code 5460 Electromag. Prop. Br.
02CY ATTN Code 2600 Tech. Library

Officer-in-Charge
Naval Surface Weapons Center
White Oak, Silver Spring, MD 20910
01CY ATTN Code WA501 Navy Nuc Prgms Off.
01CY ATTN Code WX21 Tech. Library

Commander
Naval Telecommunications Command
NAVTELCOM Headquarters
4401 Massachusetts Ave, NW
Washington, DC 20390
01CY ATTN Code 24C

Commanding Officer
Navy Underwater Sound Laboratory
Fort Trumbull
New London, CT 06320
01CY ATTN Peter Bannister
01CY ATTN D. A. Miller

Director
Strategic Systems Project Office
Navy Department
Washington, DC 20376
01CY ATTN NSP-2141

Department of the Air Force

Commander
ADC/DC
ENT AFB, CO 80912
01CY ATTN DC Mr. Long

Commander
ADCOM/XPD
ENT AFB, CO 80912
01CY ATTN XPQDQ
01CY ATTN XP

AF Geophysics Laboratory, AFSC
Hanscom AFB, MA 01731
01CY ATTN CRU S. Horowitz
01CY ATTN PHP Jules Aarons
01CY ATTN OPR James C. Ulwick
01CY OPR Alva T. Stair
02CY SUOL Research Library

AF Weapons Laboratory, AFSC
Kirtland AFB, NM 87117
02CY ATTN SUL
01CY ATTN SAS John M. Kamm
01CY ATTN DYC CAPT L. Wittwer

AFTAC
Patrick AFB, FL 32925
01CY ATTN TN
01CY ATTN TD-3
01CY ATTN TD-5
01CY ATTN TF/MAJ Wiley

Air Force Avionics Laboratory, AFSC
Wright-Patterson AFB, OH 45433
01CY ATTN AAD

Commander
Foreign Technology Division, AFSC
Wright-Patterson AFB, OH 45433
01CY ATTN ETD B. L. Ballard

HQ USAF/RD
Washington, DC 20330
01CY ATTN RDQ

Headquarters
North American Air Defense Command
1500 East Boulder
Colorado Springs, CO 80912
01CY ATTN Chief Scientist

Commander
Rome Air Development Center, AFSC
Griffiss AFB, NY 13440
01CY ATTN EMTLD Doc. Library

Commander
Rome Air Development Center, AFSC
Hanscom AFB, MA 01731
01CY ATTN EEP John Rasmussen

SAMSO/MN
Norton AFB, CA 92409
(Minuteman)
01CY ATTN NMML LTC Kennedy

Commander in Chief
Strategic Air Command
Offutt AFB, NB 68113
01CY ATTN NRT
01CY ATTN XPFS MAJ Brian G. Stephan
01CY ATTN DOK Chief Scientist

US Energy Research and Dev. Admin.

Department of Energy
Albuquerque Operations Office
P.O. Box 5400
Albuquerque, NM 87115
01CY ATTN Doc Con for D. W. Sherwood

Department of Energy
Division of Headquarters Services
Library Branch G-043
Washington, DC 20545
01CY ATTN Doc Con for Allen Labowitz

Division of Military Application
Department of Energy
Washington, DC 20545
01CY ATTN Doc Con for Donald I. Gale

University of California
Lawrence Livermore Laboratory
P.O. Box 808
Livermore, CA 94550
01CY ATTN Glenn C. Werth L-216
01CY ATTN Tech. Info Dept L-3

Los Alamos Scientific Laboratory
P.O. Box 1663
Los Alamos, NM 87545
01CY ATTN Doc Con for T. F. Taschek
01CY ATTN Doc Con for D. R. Westervelt
01CY ATTN Doc Con for P. W. Keaton
01CY ATTN Doc Con for J. H. Coon

Sandia Laboratories
Livermore Laboratory
P.O. Box 969
Livermore, CA 94550
01CY ATTN Doc Con for B. E. Murphey
01CY ATTN Doc Con for T. B. Cook ORG 8000

Sandia Laboratories
P.O. Box 5800
Albuquerque, NM 87115
01CY ATTN Doc Con for Space Proj Div
01CY ATTN Doc Con for A. D. Thornbrough ORG 1245
01CY ATTN Doc Con for W. C. Myra
01CY ATTN Doc Con for 3141 Sandia Rpt Coll

Other Government

Department of Commerce
National Bureau of Standards
Washington, DC 20234
01CY ATTN Raymond T. Moore

Department of Commerce
Office of Telecommunications
Institute for TELCOM Science
Boulder, CO 80302
01CY ATTN William F. Utlaut
01CY ATTN L. A. Berry
01CY ATTN A. Glenn Jean
01CY ATTN D. D. Crombie
01CY ATTN J. R. Wait

Department of Transportation
Office of the Secretary
TAD-44.1, Room 10402-B
400 7th Street, SW
Washington, DC 20590
01CY ATTN R. L. Lewis
01CY ATTN R. H. Doherty

Department of Defense Contractors

Aeronomy Corporation
217 S. Neil Street
Champaign, IL 61820
01CY ATTN S. A. Bowhill

Aerospace Corporation
P.O. Box 92957
Los Angeles, CA 90009
01CY ATTN Irving M. Garfunkel

Analytical Systems Engineering Corp.
5 Old Concord Rd.
Burlington, MA 01803
01CY ATTN Radio Sciences

Boeing Company, The
P.O. Box 3707
Seattle, WA 98124
01CY ATTN Glenn A. Hall
01CY ATTN J. F. Kenney

University of California
at San Diego
Marine Physical Lab of the
Scripps Institute of Oceanography
San Diego, CA 92132
01CY ATTN Henry G. Booker

Computer Sciences Corporation
P.O. Box 530
6565 Arlington Blvd
Falls Church, VA 22046
01CY ATTN D. Blumberg

University of Denver
Colorado Seminary
Denver Research Institute
P.O. Box 10127
Denver, CO 80210
01CY ATTN Donald Dubbert
01CY ATTN Herbert Rend

Develco
530 Logue Avenue
Mountain View, CA 94040
01CY ATTN L. H. Rorden

ESL, Inc.
495 Java Drive
Sunnyvale, CA 94086
01CY ATTN James Marshall

General Electric Company
Space Division
Valley Forge Space Center
Goddard Blvd King of Prussia
P.O. Box 8555
Philadelphia, PA 19101
01CY ATTN M. H. Bortner
Space Science Lab.

General Electric Company
TEMPO-Center for Advanced Studies
816 State Street
P.O. Drawer QQ
Santa Barbara, CA 93102
01CY ATTN B. Gambill
02CY ATTN DASIAC
01CY ATTN Don Chandler
01CY ATTN Warren S. Knapp

Geophysical Institute
University of Alaska
Fairbanks, AK 99701
01CY ATTN T. N. Davis
01CY ATTN Neal Brown
01CY Technical Library

GTE Sylvania, Inc.
Electronics Systems GRP
Eastern Division
77 A Street
Needham, MA 02194
01CY ATTN Marshal Cross

IIT Research Institute
10 West 35th Street
Chicago, IL 60616
01CY ATTN Technical Library

University of Illinois
Department of Electrical Engineering
Urbana, IL 61803
02CY ATTN Aeronomy Laboratory

Johns Hopkins University
Applied Physics Laboratory
Johns Hopkins Road
Laurel, MD 20810
01CY ATTN Document Librarian
01CY ATTN J. Newland
01CY P. T. Komiske

Lockheed Missiles & Space Co, Inc.
3251 Hanover Street
Palo Alto, CA 94304
01CY ATTN E. E. Gaines
01CY ATTN W. L. Imhof D/52-12
01CY ATTN J. B. Reagan D/52-12
01CY ATTN R. G. Johnson D/52-12

Lowell Research Foundation, Univ. of
450 Aiken Street
Lowell, MA 01854
01CY ATTN Dr. Bibl

M.I.T. Lincoln Laboratory
P.O. Box 73
Lexington, MA 02173
01CY ATTN Dave White
01CY ATTN J. H. Pannell L-246
01CY ATTN D. M. Towle

Mission Research Coporation
735 State Street
Santa Barbara, CA 93101
01CY ATTN R. Hendrick
01CY ATTN F. Fajen
01CY ATTN M. Scheibe
01CY ATTN J. Gilbert
01CY ATTN C. L. Longmire

Mitre Corporation
P.O. Box 208
Bedford, MA 01730
01CY ATTN G. Harding

Pacific-Sierra Research Corp.
1456 Cloverfield Blvd.
Santa Monica, CA 90404
01CY ATTN E. C. Field, Jr.

Pennsylvania State University
Ionosphere Research Laboratory
318 Electrical Engineering East
University Park, PA 16802
02CY ATTN Ionospheric Rsch Lab.

R&D Associates
P.O. Box 9695
Marina Del Rey, CA 90291
01CY ATTN Forrest Gilmore
01CY ATTN William J. Karzas
01CY ATTN Phyllis Greifinger
01CY ATTN Carl Greifinger
01CY ATTN H. A. Ory
01CY ATTN Bryan Gabbard
01CY ATTN R. P. Turco

Rand Corporation
1700 Main Street
Santa Monica, CA 90406
02CY ATTN Technical Library
01CY ATTN Cullen Crain

SRI International
333 Ravenswood Avenue
Menlo Park, CA 94025
01CY ATTN E. T. Pierce
01CY ATTN Donald Neilson
01CY ATTN George Carpenter
01CY ATTN W. G. Chestnut
01CY ATTN J. R. Peterson
01CY ATTN Gary Price

Stanford University
Radio Science Laboratory
Stanford, CA 94305
01CY ATTN R. A. Helliwell
01CY ATTN A. Fraser-Smith
01CY ATTN J. Katsufrakis

TRW Defense & Space Sys. Group
One Space Park
Redondo Beach, CA 90278
01CY ATTN Saul Altschuler
01CY ATTN Dianna Dee

Jet Propulsion Laboratory
4800 Oak Grove Drive
Pasadena, CA 91103
01 Cy ATTN: Ernest K. Smith
Mail Code: 144-B13